Dalton Transactions

ROYAL SOCIETY OF CHEMISTRY

PERSPECTIVE

View Article Online
View Journal | View Issue

Cite this: *Dalton Trans.*, 2023, **52**, 17061

Decoding the puzzle: recent breakthroughs in understanding degradation mechanisms of Li-ion batteries

Aditya Narayan Singh, *[a] Kamrul Hassan, [b] Chinna Bathula [c] and Kyung-Wan Nam *[d]

Received 11th September 2023,
Accepted 5th October 2023

DOI: 10.1039/d3dt02957c

rsc.li/dalton

Lithium-ion batteries (LIBs) remain at the forefront of energy research due to their capability to deliver high energy density. Understanding their degradation mechanism has been essential due to their rapid engagement in modern electric vehicles (EVs), where battery failure may incur huge losses to human life and property. The literature on this intimidating issue is rapidly growing and often very complex. This review strives to succinctly present current knowledge contributing to a more comprehensible understanding of the degradation mechanism. First, this review explains the fundamentals of LIBs and various degradation mechanisms. Then, the degradation mechanism of novel Li-rich cathodes, advanced characterization techniques for identifying it, and various theoretical models are presented and discussed. We emphasize that the degradation process is not only tied to the charge–discharge cycles; synthesis-induced stress also plays a vital role in catalyzing the degradation. Finally, we propose further studies on advanced battery materials that can potentially replace the layered cathodes.

1. Introduction

In the pursuit of achieving a carbon-neutral society, the contribution of lithium-ion batteries (LIBs) cannot be overlooked. LIBs have become an indispensable part of daily life and emerged as a strong candidate for replacing the fossil fuel-based economy with renewable energy sources.[1] They are now on the verge of transforming the transportation sector, and may assist in grid-storage as well. Recently, the world celebrated, with a sense of pride, the contribution to this from the Nobel laureates Stanley Whittingham, John Goodenough, and Akira Yoshino with their Nobel Prize in Chemistry in 2019.[2]

The development in understanding of the degradation mechanism in LIBs is indeed crucial for advancing and achieving a carbon-neutral society in anticipating a decarbonized grid and electrified transportation.[1,3,4] The degradation in batteries is often manifested by a reflection in capacity fading or power decay either due to mechanical or electrical origins. Furthermore, sometimes these failure origins are interconnected and make the degradation studies really cumbersome and often challenging.[5] Despite the challenges, degradation studies are essential for several reasons. Though the market growth of LIBs has reduced manufacturing costs, making LIBs last longer is crucial to a sustainable economy. The longevity of LIBs also becomes vital to ensure lifetime economies, long-term warranties, and safety, and significantly dilutes the environmental impact associated with frequent recycling–manufacturing. This study is also essential for designing novel materials meeting market requirements and accurately predicting the end-of-life (EoL) to prevent thermal runaway and save human life and property.[6] Degradation studies will not only open the door to future materials, but can also assist in improving existing commercial materials to enhance their electrochemical performances. These instances should encourage degradation studies.

It is not that degradation studies are not carried out, but they often present themselves in a complicated way. Certainly, there are some good reviews in this direction, notably a review by Demirocak's group which tries to classify the degradation mechanism in terms of chemical and mechanical modes.[7] For degradation in the anode, a review worth mentioning here is by Hapuarachchi and co-workers, who use state-of-the-art characterization techniques to describe battery failures.[8] Similarly, a few other works could be consulted (ref. 9–15).

It is worth mentioning that the degradation mechanism initiation is not always a chemical or mechanical issue; some

[a]*Department of Energy and Materials Engineering, Dongguk University-Seoul, Seoul 04620, Republic of Korea*
[b]*Advanced Energy and Electronic Materials Research Center, Dongguk University-Seoul, Seoul 04620, Republic of Korea*
[c]*Division of Electronics and Electrical Engineering, Dongguk University-Seoul, Seoul 04620, Republic of Korea*
[d]*Department of Advanced Battery Convergence Engineering, Dongguk University-Seoul, Seoul 04620, Republic of Korea. E-mail: aditya@dongguk.edu, knam@dongguk.edu*

user usage patterns also act as a catalyst to initiate it. Usage patterns like frequent charging, overcharging, deep discharging, and heating are a few scenarios that invite degradation to activate much earlier. Users should be mindful of three primary external factors that can significantly affect the degradation of batteries: working temperature, state of charge (SoC), and work/load/usage profile. The significance of each of these factors varies depending on the battery's chemistry, form, and usage history. Research by Birkl *et al.*[16] and failure models reviewed by Reniers *et al.*[17] show how these external stress factors can impact the physical degradation processes of batteries. Of these three factors, temperature is the most crucial stress factor, and any deviation from the recommended operating temperature of 25 °C can accelerate battery failure. A higher SoC can also accelerate the degradation mechanism, as electrode potential has a direct relationship with the rate of parasitic reactions occurring inside the battery, while higher current operation can increase the likelihood of failure due to mechanical stress and lithium plating during charge cycles.

Techniques that assist in characterizations are *ex situ* and *in situ* X-ray diffraction (XRD), atomic force microscopy (AFM), transmission electron microscopy (TEM), and X-ray photoelectron microscopy (XPS).

This review covers the fundamental mechanisms occurring within the manufacturer's safety limits during normal operating conditions. It also comprehensively describes the mechanisms, their consequences and interactions, experimental techniques for characterizing and triggering these mechanisms, and the state-of-the-art characterization techniques to understand them. This review also highlights the complexities of the interplay between different failure modes. Thus, coupling the interactions between various degradation mechanisms is essential to get better insights into the importance of path dependence which is often understated. Yang *et al.*[18] showed how the growth of the solid–electrolyte interphase layer leads to pore blockage and, subsequently, an increase in the rate of lithium plating,[19] ultimately resulting in a non-linear drop-off in cell capacity. Accurately capturing these complex interactions requires physics-based models instead of empirical or semi-empirical models. In this review, we also present an unbiased view of the recent progress and present the prospects for upcoming researchers to take on these challenges in their research career ahead.

2. Components and basic understanding

The mechanism of battery degradation is often a complex issue, and to better understand it, it is essential to understand what the cells are composed of and the terminologies used in batteries. For a quick overview, the major components are shown in Fig. 1. In general, the electrodes of LIBs are com-

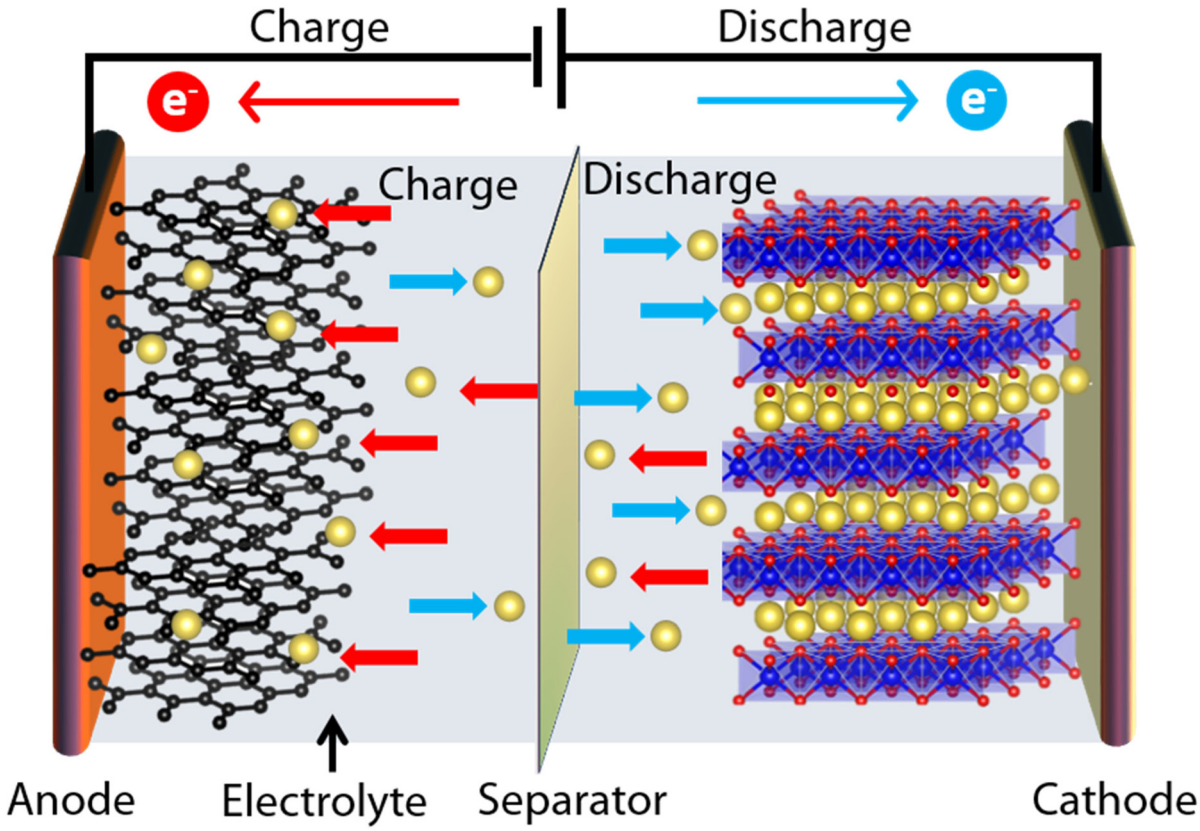

Fig. 1 Schematic representation of components used in LIB.

monly known as the anode or cathode based on their function during charge and discharge. However, since each electrode can act as either an anode or cathode, depending on whether the battery is being charged or under load (discharged), it is better to define them based on their relative electrode potentials. Thus, the electrode with the higher electrode potential, typically a lithium transition metal (TM) oxide material capable of undergoing reversible delithiation of Li^+, is referred to as the positive electrode, commonly called cathode. In general, the cathode is often a determining factor while expressing the energy-density capability of LIB. The other electrode (*i.e.*, the negative electrode), usually an intercalation material such as graphite or a graphite hybrid material, and more often lithium titanate (LTO), is commonly known as the anode.

The cathode and anode are the active materials coated on metal foils, acting as current collectors and enabling electron transport to these active materials. Before moving further, it is essential to introduce an important member of the LIB, *i.e.*, electrolytes. This is crucial, as several degradation mechanisms originate, or are at least connected to, electrodes. Depending upon their applications, the electrolyte used in LIBs may be either in the form of a liquid or a solid. Solid electrolytes are typically used in combination with gaseous or liquid electrodes. While they can be used with solid electrodes, solid-to-solid interfaces can be problematic unless the solid electrolyte is a polymer or the electrodes are thin. When a liquid electrolyte separates solid electrodes, an electrolyte-permeable separator keeps them apart. The electrolyte is responsible for conducting the ionic component of the chemical reaction between the anode and cathode, but it requires the electronic component to pass through an external circuit, where it performs electrical or useful work.

When discharging or charging a LIB, the ionic current $I_i = I$ encounters an internal battery resistance (R), causing a reduction in the output voltage (V_{dis}) from the open-circuit voltage (V_{oc}). This reduction is known as polarization and is represented by $\eta = I_{dis}R$. Similarly, during charging, the voltage V_{ch} required to reverse the chemical reaction is increased by an overvoltage $\eta = I_{ch}R$ due to the resistance R encountered by the ionic current.[3]

$$V_{dis} = V_{oc} - (q, I_{dis}) \quad (1)$$

$$V_{ch} = V_{oc} + (q, I_{ch}) \quad (2)$$

Here q is SoC, and the percentage efficiency of a cell to store energy at a constant current I is mathematically represented as:

$$100 \times \int_0^{Q_{dis}} V_{dis(q)}dq \Big/ \int_0^{Q_{Ch}} V_{Ch(q)}dq \quad (3)$$

$$Q = \int_0^{\Delta t} I dt = \int_0^{Q} dq \quad (4)$$

In the given context, Q refers to the total charge transferred per unit weight (A h kg^{-1}) or volume (A h L^{-1}) by a current $I = dq/dt$ during discharge or charge. $Q(I)$ is the cell capacity for a specific I, which depends on the rate of ion transfer across the electrode/electrolyte interfaces, becoming diffusion-limited at high currents. High-rate charge or discharge may cause a diffusion-limited loss of Li capacity, which is reversible. However, cycling can cause irreversible capacity loss due to changes in electrode volume, electrode–electrolyte chemical reactions, or electrode decomposition. The irreversible formation of a passivating solid–electrolyte interphase (SEI) layer during the initial charge of a cell in a discharged state is distinct from irreversible capacity fade that can occur during cycling. The coulombic efficiency (CE) expressed in percentage (%) for a single cycle associated with capacity fade is also essential and is represented by:

$$100 \times Q\_dis.Q\_ch. \quad (5)$$

When a LIB is being charged, the cathode is oxidized, releasing electrons to the external circuit and causing Li^+ to delithiate/remove from the cathode crystal lattice. As the Li^+ ions move across the cell and through the separator to intercalate into the layers of the anode material, electrons flow externally to the anode, reducing it and maintaining charge neutrality. Therefore, both active materials must undergo structural changes to accommodate Li^+. During discharge, the process is reversed, with the anode and cathode being oxidized and reduced, respectively. This "rocking chair" movement of Li^+ ions and electrons is necessary for charging and discharging the cell.[20] The ability to quickly and reversibly extract Li^+ from the cathode is essential and limited by the ability of the TM oxide crystal to maintain its robust crystal structure.

3. Mechanism of battery degradation

Before discussing the degradation mechanism, raising a fundamental question about the sign of degradation in batteries is essential. How does one come to know that the battery is degrading? The trivial answer to this virtually straightforward question is that no, one does not know, as one does not typically view any degradation effect during battery operation. However, the direct observable effects of degradation are capacity and voltage (power) fade.[21] Though a simple definition of decline over the time in charge that a battery can deliver can be termed a capacity fade, its mechanism is certainly not as straightforward and is highly complex. The usable capacity of a cell can be reduced through capacity fade, while power fade refers to a decrease in the deliverable power of the cell following degradation. Although these effects represent a simplified degradation perspective, they are the most measurable and frequently used practical indicators of cell deterioration.

3.1 SEI layer

In principle, the SEI is a passivation layer predominantly on anode surfaces. Generally, the SEI has similar properties to that of a solid electrolyte and is formed when the liquid electrolyte comes in contact with the electron-conductive surface

of the anode.[22] Technically it is formed by the irreversible electrochemical decomposition of the electrolytes and thus contains the properties of electrolytes (Fig. 2). The SEI layers themselves are repellent to electrolyte and do not allow electrolyte penetration, thus protecting the anode from further reacting to the electrolyte. In short, the SEI acts as a protective layer to the anode. However, the working voltage of the SEI lies below the electrochemical stability window of the electrolyte,[23] which causes an irreversible breaking down of the electrolyte and accelerating of redox processes, leading to a severe loss of electrolyte. The published literature highlights that Li metal electrodes and graphite develop this SEI layer.[24,25] Numerous compounds have been observed within the SEI, such as lithium fluoride (LiF), lithium carbonate (Li_2CO_3), lithium oxide (Li_2O), lithium methyl carbonate ($LiOCO_2CH_3$), and lithium ethylene dicarbonate ($LiOCO_2CH_2)_2$.[26] The SEI layer quickly forms (depending upon C-rate) on the first cycle of the cell, resulting in *ca.* 10% reduction in capacity, but then serves to restrict any further reaction of the electrolyte at the anode, thus protecting it against further deterioration. However, the thickness of the SEI layer increases (predominantly on the graphite anode) as the cell ages. The growth in the SEI layer could be due to several reasons, including diffusion of solvent molecules through the existing SEI and newly exposed electrode surfaces, which result from cracking and deposition of side reaction products,[27] such as plated Li and TM ions dissolved from the cathode, which react with the electrolyte to form the SEI. The fractional capacity loss is associated with the SEI growth rate, which approximately correlates with the square root of time;[28,29] as the SEI thickness increases, the rate of solvent molecule diffusion slows down.

The formation of the SEI commences upon lithiation of the anode and its exposure to the electrolyte, and continues to grow even when the battery is idle. However, the growth rate of the SEI is accelerated by high temperatures due to increased diffusion rates. Furthermore, high currents can cause particle cracking (due to the generation of a greater stress profile) and initiate the formation of a new SEI layer. Although LTO anodes are generally stable with most organic electrolytes and do not typically form an SEI layer under normal conditions, an SEI layer can still form at potentials below 1 V, though in a single crystal it is estimated to form at ~1.8 V *vs.* Li/Li^+ as well.[30] The loss of capacity in batteries occurs due to the irreversible entrapment of otherwise recyclable lithium within the SEI layer. Additionally, the SEI layer is less permeable to Li^+ than the electrolyte, which results in pore blocking and a decrease in electrolyte flow, further compounded by the consumption of the electrolyte solvent. These cumulative effects lead to an increase in cell impedance and power fade. Although the SEI layer is not directly linked to catastrophic battery failure, at higher temperatures, it can decompose and contribute to thermal runaway events.[31] Moreover, SEI growth reduces the amount and conductivity of the electrolyte as it consumes the electrolyte solvents.

As mentioned earlier, the degradation mechanism in batteries is not always due to a prime culprit, but may be due to combinations of, or linked to other, mechanisms as well. Here we highlight how the SEI layer can further aggravate the situation and degrade the battery performance further. Essentially, the TM ions dissolved from the cathode (a mechanism well known as TM dissolution[32]) are deposited on the anode, accelerating SEI growth.[33] Additionally, particle and SEI cracking, caused by high cycling rates and significant volume changes, open up new surfaces for new SEI formation. Furthermore, plated Li can undergo additional side reactions with the electrolyte to form more SEI. Loss of lithium inven-

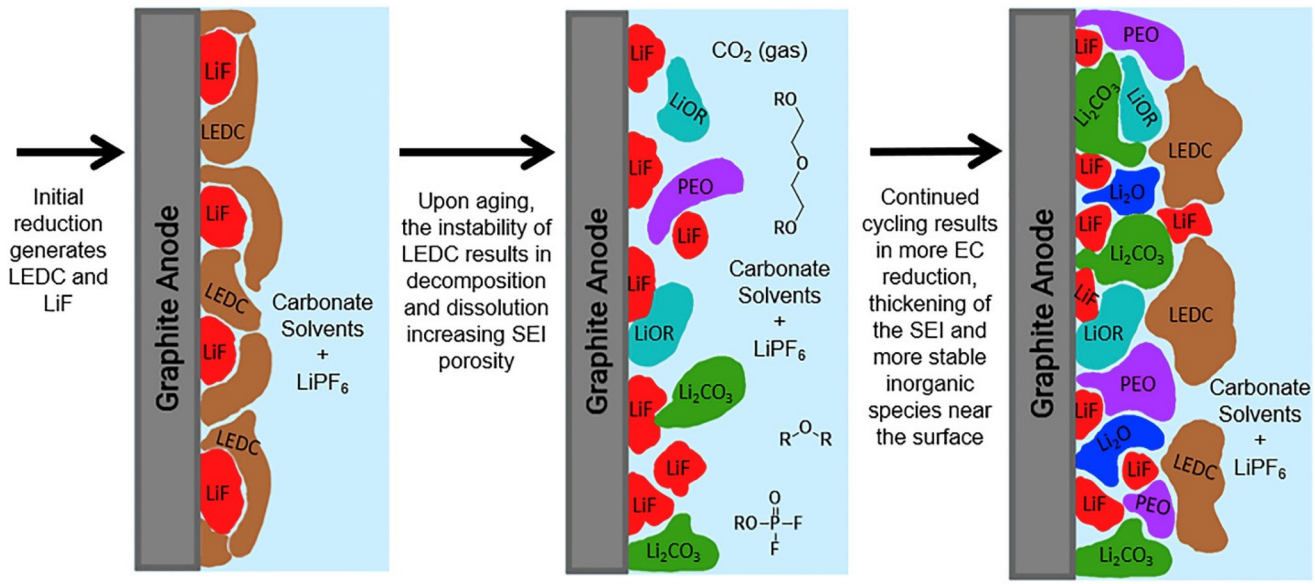

Fig. 2 Schematic representation of SEI formations on the anode and its thickening during continued cycling. During initial reductions, ethylene carbonate (EC) yields lithium ethylene dicarbonate (LEDC) and ethylene, reproduced from ref. 25 with permission from Elsevier, Copyright 2019.

tory from the anode causes the electrodes to become imbalanced relative to each other, causing stoichiometric drift, which can lead to excessive de-lithiation and accelerated degradation of the cathode at high SoCs.

3.2 CEI

Although significant progress has been made on the electrode–electrolyte interphase (EEI) and SEI, fewer efforts have been made to understand the cathode–electrolyte interphase (CEI) chemistry. Fig. 3 quickly summarizes the history and recent progress on the CEI in the last decade. In 1979, Peled[34] initially reported that alkali metals react with non-aqueous electrolytes in non-aqueous battery systems, forming an insoluble product layer. This layer acts as an interphase between the metal and the solution, exhibiting solid electrolyte characteristics that hinder electron conductivity. Consequently, it is referred to as the SEI. Later in 1985, Goodenough and co-workers[35] observed the development of a polymer interphase similar to the SEI on the surface of $LiCoO_2$ cathode material. Subsequent investigations further explored this phenomenon that the CEI can be formed on various other cathode surfaces with general representation $LiTMO_2$ (TM: Ni/Co/Mn), and Li must shuttle through the CEI during the dissolution/intercalation process.[36] These discoveries about the CEI also led to the birth of several hypotheses during the early days. For example, a very popular one was the nucleophilic reaction of the $LiNiO_2$ electrode and the surface ion exchange of the $LiMn_2O_4$ electrode as proposed by Aurbach in 2000.[37] According to Aurbach, the highly reactive nucleophilic oxide $LiNiO_2$ can react with CO_2 in the presence of air, forming a Li_2CO_3 layer. This reaction product replaces the original surface and forms film rich in $ROCO_2Li$, where R represents a carbon and hydrogen atom group of varying sizes. On the other hand, $LiMn_2O_4$ has low nucleophilicity and exhibits limited surface reactivity towards solvent molecules or anions. However, it can exchange with hydrogen ions, leading to the formation of an inactive surface layer. Subsequent research revealed that the composition of cathode materials, electrolytes, solvents, salts, and additives all influence the formation of the CEI.

It is generally believed that CEI formation is attributed to the formation of the electrochemical oxidation and decomposition reactions of the electrolyte occurring on the cathode surface. In 2013, Goodenough and Park incorporated Kenichi Fukui's frontier orbital theory into the electrochemical reaction process (Fig. 3a) to explain the formation mechanism of the EEI.[3] Additionally, the formation process of the CEI is believed to be interconnected with the dynamic evolution of the SEI on the anode side. As illustrated in Fig. 3b, SEI fragments detached from the anode migrate through the electrolyte to the cathode and actively participate in the creation of the cathode CEI.[38] This hypothesis has been further validated in subsequent studies conducted by other researchers.[39,40] The CEI and its associated mechanism can be better studied by advanced characterization techniques. The X-ray absorption spectroscopy (XAS) technique was employed to reveal the dynamic changes in CEI of a Li-excess cathode $Li_{1.2}Ni_{0.15}Co_{0.1}Mn_{0.55}O_2$ (Fig. 3c). The normalized X-ray absorption near-edge spectra (XANES) and Fourier-transformed spectra of the cathode surface display a few exciting findings. When the voltage remains below 4.4 V, the Ni K-edge spectrum shows a continuous shift towards higher energy, suggesting the oxidation of Ni^{2+} towards Ni^{4+}. However, minimal changes are observed at the 4.4 V plateau, indicating limited further oxidation of Ni within this voltage range. On the other hand, the shape of the Mn and Co K-edge spectra changes gradually as the voltage increases while the absorption edge position remains constant. This phenomenon is attributed to local structural changes during the lithium deintercalation process.[41] Moreover, Fourier transform spectroscopy reveals that the Ni–O and Co–O peaks exhibit slight variation beyond 4.4 V, whereas the Mn–O peak intensity increases. This outcome indicates that the non-platform area observed during the initial charging primarily corresponds to the oxidation of Ni and Co, while the voltage platform region is associated with Mn. Further improvements in revealing the surface chemistries of $LiNi_{0.7}Co_{0.15}Mn_{0.15}O_2$ were obtained by adopting a mosaic-like model given by Manthiram and co-workers (Fig. 3d and e).[42] This study revealed that tuning the interphase thickness is a handy tool to regulate the deterioration of the electrode–electrolyte interface, particularly during high-voltage operation. It is essential to mention here that during characterization in air, the CEI can meet side reactions; thus, care must be taken to restrict the side reactions. Cryo-TEM imaging is one such non-destructive technique that can bring a wealth of information on the CEI, with its non-destructive nature and ability to preserve the chemistry intact during characterization at temperatures close to ~103 K. Alvarado *et al.*[43] conducted an interesting study on the CEI in different electrolytes, which revealed that a carbonate-based electrolyte possesses a poor and non-uniform formation of the CEI; conversely, when using LiFSI-sulfolane, the CEI coverage demonstrates a more uniform distribution (Fig. 3f). Quantum chemistry (QC) calculations predict that high salt concentrations under oxidative conditions promote complex/aggregate formation, which retards the decomposition of sulfolane and leads to the production of polymerizable products instead of gaseous ones, which brings a notable improvement over carbonate solvents. Apart from the solvent's influence, the presence of a high-concentration electrolyte can alter the frontline orbital properties and solvation structure of lithium ions within the electrolyte. Consequently, this modification can impact the interface reaction between the electrode and electrolyte.[44,45] Despite several improvements in understanding the chemistry of the electrolyte to optimize battery performance, a truly functional electrolyte seen from the commercial point of view is still tricky to find. In this context, a localized high-concentration electrolyte (LHCE) is formulated, which has good cathodic but poor anodic stability, to carefully build a protective interphase on both the anode and cathode simultaneously.[46] As shown in Fig. 3g, the formation of a CEI rich in inorganic components such as LiF, S–O_x, and N–O_x primarily arises from the decomposition of LiFSI and TTE, respectively. Despite continu-

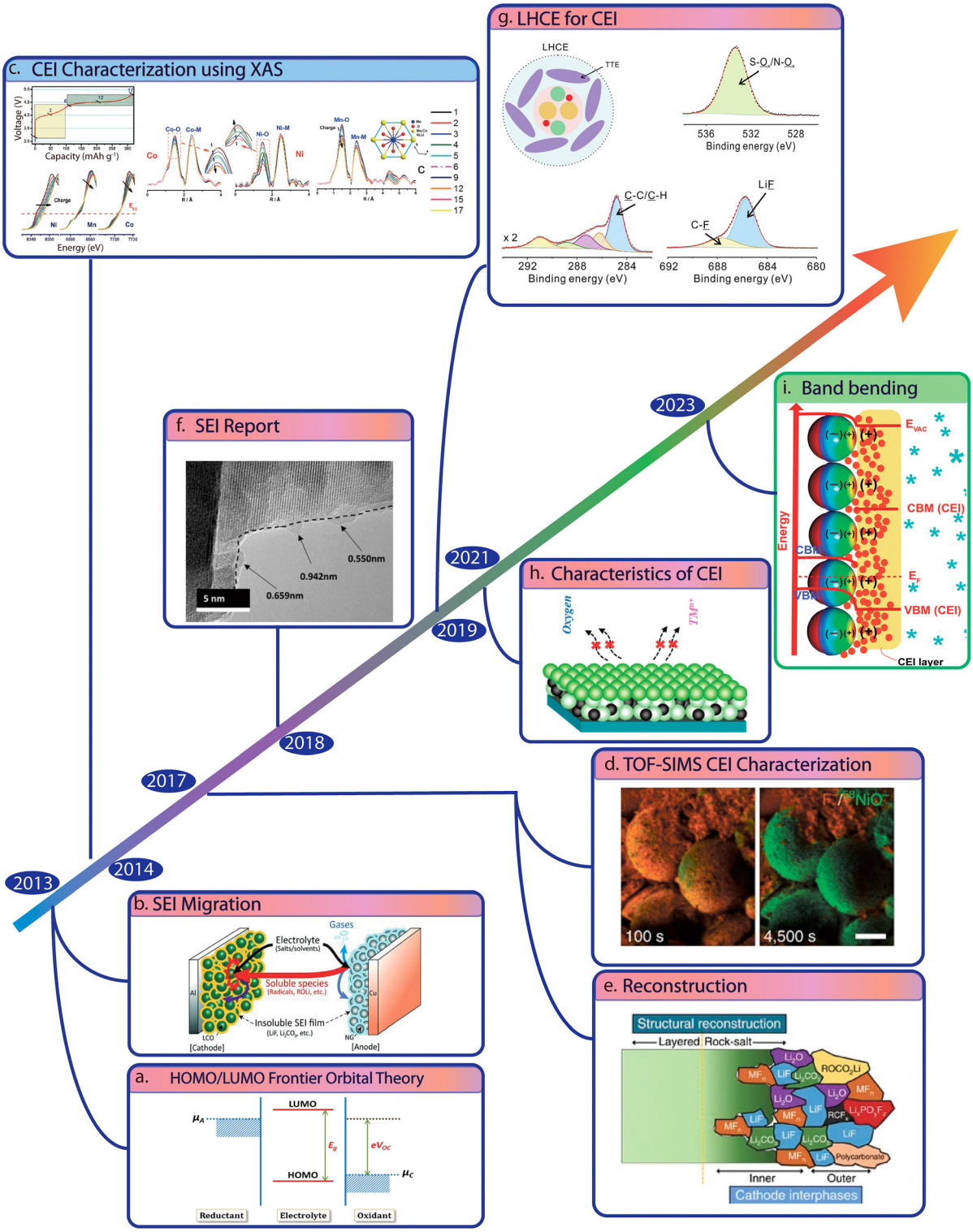

Fig. 3 Progress timeline of the CEI in the previous ten years (2013–2023). (a) The relative potential of the electrode and electrochemical stability window of the electrolyte. Reproduced from ref. 3 with permission from the ACS, copyright 2013. (b) Reductive decomposition of SEI and participating in the formation of CEI. Reproduced from ref. 38 with permission from John Wiley and Sons, copyright 2013. (c) The *in situ* characterizations of CEI using XAS. Reproduced from ref. 51 with permission from John Wiley and Sons copyright 2014. (d) TOF-SIMS characterization of CEI. (e) A mosaic diagram of the surface degradation products of cycled $LiNi_{0.7}Mn_{0.15}Co_{0.15}O_2$. Reproduced from ref. 42 under CC license 4.0. (f) Cryo-TEM image of CEI. Reproduced from ref. 43 with permission from Elsevier, copyright 2018. (g) Solvated structure of LHCE. Reproduced from ref. 46 with permission from Elsevier, copyright 2019. (h) Defining characteristics of CEI. Reproduced from ref. 47 with permission from Elsevier, copyright 2021. (i) Schematic diagram showing band bending with CEI. Reproduced from ref. 50 with permission from the RSC, copyright 2023.

ous advancements in understanding the CEI, comprehending it fully remains challenging due to the complex nature of interface reactions. However, redesigning ether-based LHCE can significantly arrest side reactions and improve electrochemical performances under a satisfactory cut-off voltage of ~4.5 V.

Several seminal efforts have been made to develop a robust CEI by engaging film-forming electrolytes. The primary goals of these endeavors have been to impede parasitic reactions with the electrolyte and effectively control phase transitions at normal temperatures. However, fewer studies have emphasized enhancing the thermal stability of the CEI. It is essential to highlight that the characteristics of the CEI (Fig. 3h) should encompass electrochemical, mechanical, chemical, and thermal stability.[47–49] It is also necessary to mention here that a phenomenon that has not been taken into consideration is band bending.[50]

Band bending is a significant phenomenon that occurs at the interface between materials with different band gaps, such as the cathode material and electrolyte in LIBs. During charging, lithium ions are inserted into the cathode, causing the Fermi level of the cathode to shift upward until it aligns with the conduction band minimum of the electrolyte, resulting in band bending. This process has crucial implications for battery performance. It helps stabilize the cathode by preventing the diffusion of lithium ions out of it and facilitates the extraction of lithium ions during discharge. The extent of band bending can be influenced by factors like the cathode material's band gap, the electrolyte's dielectric constant, and the surface morphology of the cathode material. Understanding and manipulating band bending could contribute to the design of more efficient cathode materials and electrolytes, leading to improved LIB performance.[52]

3.3 Lithium plating

The origin of the term "metal plating" can be traced back to the 1800s,[53,54] when homogeneous metal coatings were first reported. At that time, metallic needles were deposited on a silver wire, and silver medals were plated with gold.[55] Today, metal plating is commonly used to form closed films on surfaces for protection and to give them novel properties.[56,57] Sadly, Li deposition or plating on anodes of LIBs can lead to fast degradation, corrosion, and several safety-related issues and is therefore not recommended. A detailed understanding of the underlying mechanism is essential to prevent Li deposition or plating. This understanding is also crucial as several performance parameters are connected to Li metal plating/deposition (Fig. 4a). Although the term "metal plating" is often used in the literature on LIBs,[58–61] it is unclear whether the deposited Li film is homogeneous or not. Recent studies have revealed that Li metal can be deposited in various macroscopic morphologies.[62–64] Therefore, the terms "Li plating" and "Li deposition" have been defined based on the morphologies found in commercial LIBs, as shown in Fig. 4b. The term "Li deposition" is the general term that may be used for all kinds of morphologies, including "Li plating", "local deposition", or "marginal deposition". It is important to note that the difference between plating and deposition is not the dendritic growth.

Li is removed from the cathode when charging the LIB and transported as Li^+ ions through the electrolyte to the anode, where it is typically intercalated into graphite particles. Li deposition on graphite anodes is possible under thermodynamic conditions, but it is not a competitive reaction compared with Li insertion. However, during high C-rate charging, the process is not in equilibrium, and polarization is mainly caused by overpotential promoting Li deposition. The overpotential can be calculated in simulations and is used as the kinetic condition for Li deposition. When the sum of the equilibrium potential and overpotential is negative *vs.* Li/Li^+, Li deposition occurs, similar to measuring a negative anode potential in a 3-electrode cell with a reference electrode.

Before moving to other discussions, it is essential to look at Fig. 4c. It can be inferred from the chart that these studies are gaining equal attention as designing novel electrodes, marked by numerous publications. Interestingly, very few researchers have undertaken extremely low/high temperature and high C-rates studies, and a majority of them have concentrated on room temperature with 1 C-rate studies. This necessitates, and

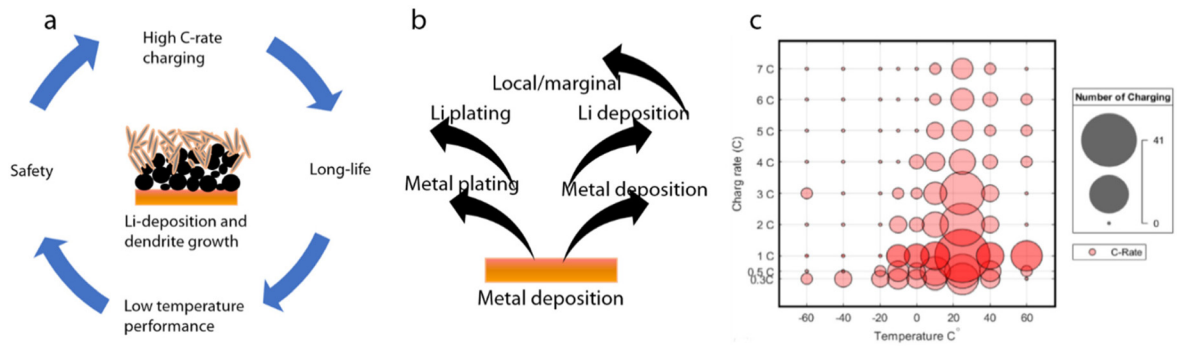

Fig. 4 (a) Schematic representation of Li-deposition and its interactions. (b) Metal deposition and its various terminologies. (c) Summary of available literature data based on C-rates and temperatures. The larger size of the dots represents a larger number of publications considering C-rates at that particular junction. Reproduced from ref. 19 with permission from Elsevier, copyright 2021.

indeed invites, upcoming researchers to carry out studies at extreme temperatures with high C-rates.

3.4 Structural changes in the cathode

It is important to understand that electrochemical performance is deeply tied to the structural properties, often known as structure–property relationships.[65] Maintaining long-term structural stability is essential in batteries and is one of the essential requirements in almost all energy conversion reactions.[65–69] Thus, addressing the structural stability in batteries becomes of prime importance to ensure long-term performance.

The cathode is one of the main components of a rechargeable battery, and its structure can change during its operation. One of the most common changes is the degradation of the cathode material, which can occur due to repeated charging and discharging cycles. During these cycles, the cathode material can undergo structural changes such as cracking, phase changes, or dissolution of the active material. These changes can decrease the battery's specific capacity and performance over time. For example, in a LIB, the layered cathode material typically consists of lithium metal oxides, such as lithium cobalt oxide (LCO), olivine type as lithium iron phosphate (LFP), or spinel structure as lithium manganese oxide (LMO). During cycling, the lithium ions move back and forth between the cathode and anode, and the cathode material can undergo structural changes due to the insertion and extraction of these ions. One common degradation mechanism in LCO cathodes is the formation of a spinel phase, which can reduce the material's capacity and stability. In LFP cathodes, the formation of a surface layer of lithium phosphate can decrease the electrode's conductivity and affect the battery's overall performance. To mitigate these structural changes and extend the battery's lifespan, researchers are exploring new cathode materials and designs that can improve the battery's stability and cycling performance. Amid a long list of TM-based compounds used in LIBs as cathodes, including layered materials such as $LiCoO_2$, $LiNi_xCo_yMnzO_2$, spinels, polyanions, and Li-rich, we focus on a few of the essential ones here. The ongoing discussions explain the mechanism of structural degradation in Li-rich layered oxide cathode.[70] During the charge–discharge process in $Li_{1.16}Ni_{0.19}Co_{0.19}Mn_{0.46}O_2$, there is a structural change that increases the amount of low-valent manganese (Mn) and nickel (Ni) ions in the lithium (Li) layer (Fig. 5).

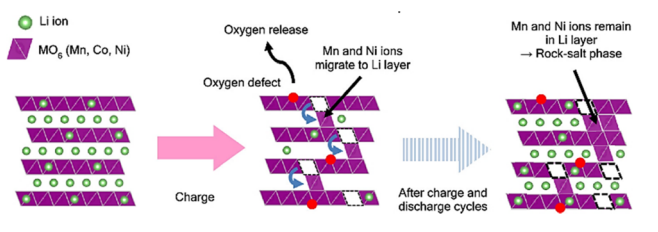

Fig. 5 Mechanism of structural degradation in Li-rich layered cathode at the surface forming rocksalt phase. Reproduced from ref. 70 with permission from the ACS, copyright 2019.

Additionally, the proportion of divalent manganese, cobalt (Co), and nickel ions increases on the surface of the active materials. In a portion of the surface of the active material, these migrated Mn and Ni ions do not return to the TM layer during discharge but instead remain in the Li layer. As a result, the Mn and Ni ions in the Li layer can replace the original Li ions in the crystal lattice, leading to a rocksalt-type structure of metal monoxides. The valence states of the Mn and Ni ions at the surface, as determined by s-XAS (synchrotron X-ray absorption spectroscopy), are found to be similar to those of MnO and NiO in the rocksalt-type structure. Specifically, the s-XAS results suggest that the Mn and Ni ions at the surface are divalent (Mn^{2+} and Ni^{2+}). This indicates that the charge–discharge cycle induces a structural change in the battery's active material, where the proportions of divalent Mn, Co, and Ni ions increase at the surface of the active material. Thus, it is clear that the charge–discharge process can induce structural changes from the layered to rocksalt phase, which are irreversible. This irreversible phase is deleterious to cathode materials and often results in the underperformance of LIB.

3.5 Cycling-induced particle fracture

The fracturing of particles happens in electrodes due to the significant change in the volume of the electrode materials and the resulting stress that occurs during electrochemical operation. Quite recently, it has been found that it is not only the cycling-induced stress that needs to be blamed for the particle fracture, but the synthesis-induced stress is the key player which initiates such failures during cycling.[71] Though explaining such a mechanistic study is not the key idea of this review, it is advised to refer to ref. 72 and 73. There are several sites from which particle fragmentation may initiate. For example, the cause of particle fragmentation near the separator is due to higher local current densities causing more considerable stresses. Furthermore, the degree of particle fragmentation is influenced by the mechanical characteristics of the material and is primarily determined by the magnitude of the volume alterations caused by the charging and discharging processes.[74] When subjected to high current density and a broad range of voltages during the cycle process, micro-cracks are more likely to form in the electrode material, leading to performance degradation. Elevated temperatures can also expedite the side reactions between the electrode and the electrolyte.[75] Typically, the fragmented section loses contact with the current collector or the remaining active material. Furthermore, the newly exposed surface becomes a reaction site for the electrolyte, causing the creation of an imperfect SEI film. As the SEI film is not generated during the optimized initial charge/discharge conditions, its quality is often lower. The imperfect SEI film in LIBs can consume the limited lithium inventory and inhibit the transport of electrons and lithium ions, leading to further performance degradation.[76,77]

Before discussing how to characterize several degradations in LIBs, we summarize several mechanisms by which electrochemical performances are hampered (Fig. 6). Though the illustrated figure concerns taking $Li_xMn_2O_4$ as an example, it

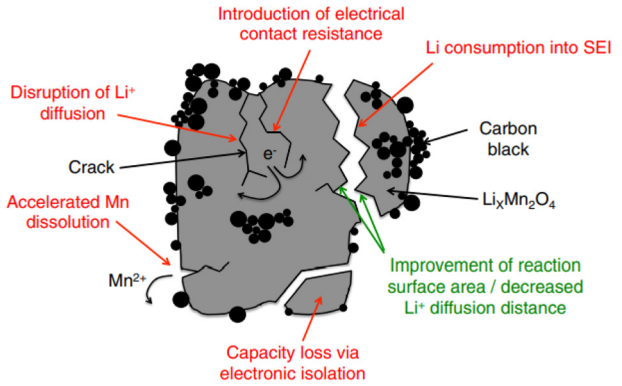

Fig. 6 Schematics showing the mechanism by which fracture in LIB can impact performance. Reproduced from ref. 78 with permission from IOP Publishing, copyright 2017.

can be applied to almost all the cathode materials used in LIBs.[78]

Efforts to understand the root cause of particle fracture and the associated performance degradation must be considered at the forefront of battery research to improve the electrochemical performances of LIBs. The development of advanced *ex/in situ* characterization techniques, including transmission electron microscopy (TEM) and *in situ* X-ray transmission microscopy (TXM), have assisted in exploring the crystal structure and morphology changes of active materials during the electrochemical cycle. Computation models have also been used to study the complex degradation mechanism caused by particle fracture.

3.6 Dissolution of TMs from the cathode

Though several processes occur at the cathode/electrolyte interface, here we are much more interested in the critical failure mechanism: the dissolution of TMs from the cathode. The dissolution mechanism is driven by the formation of TMs in their respective ionic states due to the oxidizing capability of the electrolytes' weak acid-like feature, which consists of a mixture of organic solvents and lithium salts.[79] In addition to this primary reason, several other factors, such as high-voltage operation, lead to oxidative reactions, causing the release of TM ions from the cathode material.[80] Electrolyte decomposition at high voltages generates reactive species that attack the cathode, promoting transition metal dissolution.[81] Surface reactions, such as oxygen evolution or SEI layer formation, create chemical environments that encourage dissolution.[82] Crystal lattice instability in certain cathode materials due to charge/discharge cycles results in the degradation of the crystal structure and subsequent dissolution.[83] Some cathode materials lack a protective surface passivation layer, increasing susceptibility to dissolution.[84] Understanding and managing these factors is crucial for reducing transition metal dissolution and improving battery performance.

The dissolution model, particularly Mn from $LiMn_2O_4$ (LMO), was proposed by Gummow *et al.*[85] in an acidic aqueous medium such as $LiMn_2O_4 + 4H^+ \leftrightarrow 2Li^+ + Mn^{2+} + 3\lambda\text{-}MnO_2 + 2H_2O$. Though there is no consensus that this reaction mechanism still holds good in non-aqueous systems, the Mn^{2+} ions generated during the dissolution strongly react with other carbonate solvent molecules and electrolyte anions, resulting in Mn complexes. These Mn complexes then get deposited onto the SEI of the anode, often responsible for cell degradation. Analysis using scanning electrochemical microscopy (SECM) revealed that the dissolution of Mn from LMO was accelerated by holding (5 h) the cathode at 4.5 V *vs.* Li/Li^+. Analysis of the SECM voltage hold samples by inductively coupled plasma (ICP) and electron paramagnetic resonance (EPR) revealed that 0.5 mg L^{-1} Mn was found in the electrolyte sample, indicating the occurrence of Mn release from the LMO electrode. On Mn^{3+}, EPR remains silent as reflected in larger zero-field splitting; however, both Mn^{2+} ($3d^3$) and Mn^{4+} ($3d^3$) remain EPR active at X-ray band frequency (9.38 GHz) in the electrolyte sample. However, EPR remains substantially silent on Mn^{4+} in voltage-hold SECM cells. It is now essential to state that the degradation of the LMO cathode is influenced by several factors, of which the presence of lithium salts and varying hold time during charging impact severely. To explore this, several voltage-hold experiments varying the tip positions in electrolytes, namely $LiClO_4$, $LiPF_6$, and LiTFSI (bis(trifluoromethanesulfonyl)imide), were conducted (Fig. 7a). The cyclic voltammetry (CV) analysis of both $LiClO_4$ and $LiPF_6$ electrolytes after a 5 h voltage hold reveals clear signals indicating the presence of electroactive degradation products (Fig. 7b). Interestingly, the CV of the $LiPF_6$-based electrolyte shows a similar trend to that of the $LiClO_4$ electrolyte, exhibiting an oxidation/reduction peak at ~3.3/3.2 V, respectively. However, unlike the $LiClO_4$ electrolyte, the CV of the $LiPF_6$-containing electrolyte lacks the asymmetry observed in its counterpart. The $LiPF_6$-containing electrolyte displays a noteworthy characteristic where the peak reduction current at 3.2 V almost matches the peak oxidation current at approximately 3.3 V. This observation suggests that the formation of the manganese (Mn) complex in the presence of PF_6^- anions may confer greater stability in terms of electrochemical or solution-based reactivity. Additionally, the CV of the $LiPF_6$-based sample exhibits an additional redox process above 4.5 V, displaying irreversible behavior. In contrast, the $TFSI^-$-containing electrolyte presents distinct features in the voltammogram obtained after the 5 h voltage hold. These characteristics are different from those observed in electrolytes containing PF_6^- and ClO_4^- anions. The inclusion of PF_6^- and ClO_4^- anions noticeably enhances the dissolution of Mn, possibly by generating acid through processes such as the hydrolysis of PF_6^- to produce HF or the oxidation of ClO_4^- to yield HCl. When compared with electrolytes that solely contain the $TFSI^-$ anion, there is still Mn dissolution, but at a significantly slower rate, and this difference is due to the absence of acid generation potential in the $TFSI^-$ system. In a recent study it has been reported that the formation of the CEI is a dynamic process. Throughout the electrochemical reaction, the CEI is continually and reversibly generated and dissolved, leading to the continual consump-

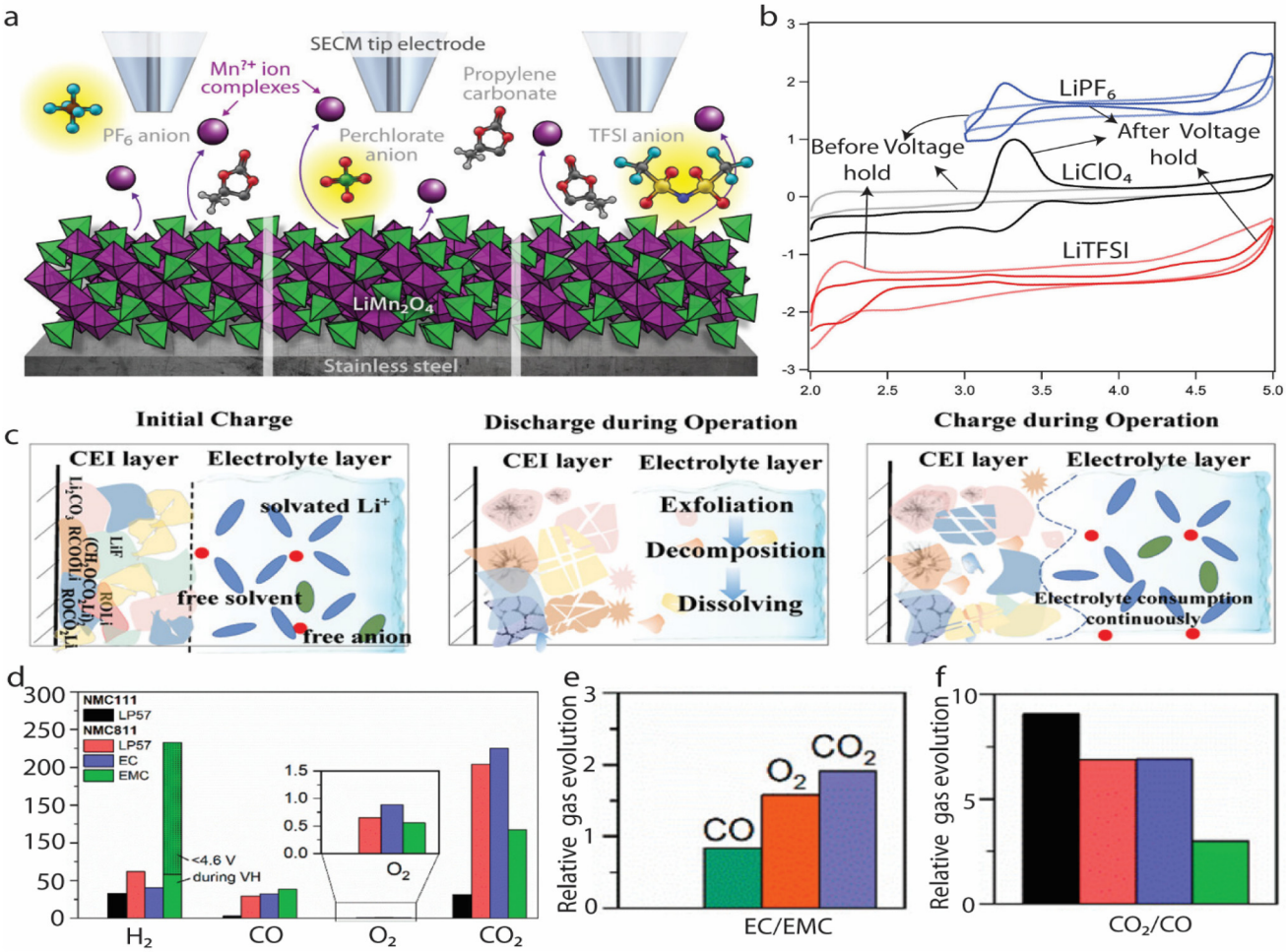

Fig. 7 (a) Schematic diagram showing various dissolutions at CEI and SECM electrodes to probe them. (b) A normalized SECM graph collected for the LMO electrode on Stainless steel. Reproduced from ref. 79 with permission from the ACS, copyright 2021. (c) Schematic diagram depicting the dynamic evolution of CEIs during charge–discharge operations. Reproduced from ref. 87 with permission from John Wiley and Sons, copyright 2022. (d) Online electrochemical mass spectroscopy (OEMS) data showing the quantity of H_2, CO, O_2, and CO_2 and a magnified view of O_2 (inset). (e) Relative gas evolution observed in NCM811 in EC/EMC electrolyte with 1.5M $LiPF_6$. (f) The relative fraction of CO_2/CO for NMC-electrolyte full cell configuration using LTO. Reproduced from ref. 88 with permission from the ACS, copyright 2022.

tion of the electrolyte.[86] Liu's group recently reported the dynamic evolution of the CEI on the surface of NCM811 as observed under *in situ* FTIR (Fig. 7c).[87] The intensity of various species such as LiF, RCOOLi, $(CH_2OCO_2Li)_2$, Li_2CO_3, and ROCOOLi demonstrates an upward trend as the potential increases. Conversely, these peaks exhibit a continuous decrease during discharge. This dynamic and reversible transformation of the CEI corresponds to the generating/disappearing/regenerating of EC. Consequently, the development of the CEI on the cathode surface adheres to a pattern of generation, exfoliation, dissolution, and regeneration. Strikingly, this interfacial reactivity increases further in Ni-rich cathodes than in their lower Ni-content counterpart. An extensive study on charged NMC111 and NMC811 was undertaken to establish this idea.[88] Interestingly, in a full cell configuration using $Li_4Ti_5O_{12}$ (anode), NMC111 exhibits similar parasitic currents under both EC-containing and EC-free electrolytes during high voltage holds. However, this is not the case for NMC811 under a similar condition (Fig. 7d). Furthermore, online gas analysis reveals that the solvent-dependent reactivity for Ni-rich cathodes is related to the extent of lattice oxygen release and accompanying electrolyte decomposition, which is higher for EC-containing than EC-free electrolytes. The presence of EC-containing electrolytes leads to increased lattice oxygen release, resulting in higher cathode interfacial impedance, a thicker surface reconstruction layer with oxygen deficiencies, greater electrolyte solvent and salt breakdown, and increased dissolution of TMs. In contrast, these processes are suppressed in EC-free electrolytes. These findings underscore the incompatibility between conventional electrolyte solvents and Ni-rich cathodes. In addition to the NCM and LCO,[39] CEI dissolution is also reported on the surface of $LiNi_{0.5}Mn_{1.5}O_4$.[89] The CEI study on high-voltage spinel $LiNi_{0.5}Mn_{1.5}O_4$ reveals that the CEI is susceptible to corrosive acidic species, particularly HF,

which is generated during electrolyte oxidation. HF damages the CEI by leaching out inorganic components like LiF and $Li_xPO_yF_z$. However, when Al_2O_3 is introduced as an HF scavenger, the CEI remains relatively stable, leading to a significant improvement in CE. These findings highlight the influence of HF on the partial dissolution of the CEI and the additional role of Al_2O_3 in facilitating CEI deposition.

These discussions highlight the importance of stabilizing the CEI for obtaining improved electrochemical performances. Thus judicious efforts must be taken to modify the CEI to have stable electrochemical performances.

3.7 Methods to modify the CEI

Increasing the charge cutoff voltage is a highly effective approach for addressing the need for high specific capacity and energy density in batteries. However, this process encounters several challenges, including accelerated crystal structure degradation, deterioration of interfaces, dissolution of TM ions, electrolyte decomposition, cathode phase transition, particle fragmentation, and oxygen release. These issues contribute to an increase in cathode impedance and voltage decay. The presence of a uniformly distributed and stable CEI is crucial for proper battery operation. The structural stability and mechanical properties of the CEI can be altered in two primary ways: through modifications on the electrolyte side, particularly the interfacial hybrid layer (IHL), and on the electrode side, involving the choice of materials. Researchers have predominantly focused on enhancing the CEI by optimizing the electrolyte system using electrolyte additives, LHCEs, solid-state electrolytes, artificial CEI formation, cation doping, and other strategies. These approaches aim to inhibit detrimental interphase reactions and promote the smooth migration of ions within the battery system.

3.7.1 Electrolyte engineering. Sacrificial electrolyte additives provide a straightforward and cost-effective approach compared with other existing strategies for optimization of the CEI. These additives, possessing higher HOMO values than solvents and other components, can undergo preferential decomposition on the cathode surface. The distinct structure and function of sacrificial additives contribute to stabilizing electrochemical oxidation at the interface, forming a CEI layer with enhanced ionic conductivity and favorable chemical/electrochemical stability. Although these additives are in minimal quantities, they cannot completely replace the electrolyte decomposition process. Nonetheless, by being uniformly dispersed throughout the electrolyte, the additive can modulate the formation process and elemental composition of the CEI.[90] There are numerous classes of additives, such as boron-,[91] nitrogen-,[92] phosphorous-,[93] fluorine-,[94] and silicon-containing additives.[95] Though there may be several other classifications available such as inorganic and organic-based additives, they all have common attributes. Ideally, any additive should be capable of selectively decomposing on the cathode surface, facilitating the creation of a stable and uniform CEI. This preferential decomposition forms a CEI that exhibits excellent stability and homogeneity. Recently, studies revealed that a uniform and thin film was selectively generated on the cathode surface by incorporating 2 wt% trimethyl borate (TMB) with enhanced oxidation activity into the base electrolyte.[96] This electrophilic layer, originating from the boron substrate on the CEI, effectively captured the superoxide anion species and enhanced the structural stability and performance of the electrode. Likewise, another boron-containing composite, utilizing methylboronic acid MIDA ester (ADM) with 1 wt% boron–nitrogen–oxygen alkyl groups, exhibited notable characteristics such as high capacity retention and rate capability.[97] Currently, lithium bis(oxalato)borate (LiBOB) stands as the extensively researched borate additive. In conventional ester-based electrolytes like EC and ethyl methyl carbonate, the surfaces of NCM particles exhibit a significantly disordered layer along with a rock salt phase (NiO), resulting in poor surface structure stability. LiBOB undergoes oxidation at approximately 4.2 V (*vs.* Li+/Li) and can decompose to form a CEI layer that predominantly contains borate components.[98] In contrast, the cathode particles do not exhibit any visible rock salt phase on their surfaces. Notably, the amount of B component (BO^-) in the CEI shows a significant increase, while the presence of interphase substances such as C_2HO^-, PO_2^-, and POF_2^- weakens. The combination of LiBOB and oxygen radicals favors the formation of a boron-rich layer that includes oxalate, lithium fluoride, and alkyl borate. This boron-rich layer acts as a stabilizing element, enhancing the stability of the protective CEI layer on the cathode and reducing the dissolution of TM ions.[99] Similarly, Ni-rich cathodes, despite their ability to deliver high energy density, suffer from structural instabilities at high voltage operations (>4.3 V). To reinforce structural stabilities, the inclusion of LiBOB has shown significant improvements in cycling stability, with a remarkable capacity retention of 81.7%. Notably, even after 200 cycles at 1C rate, minimal voltage hysteresis is observed.[100] This exceptional electrochemical performance can be attributed to an enhanced structural and interfacial stability, achieved by mitigating the formation of micro-cracks and surface degradation during cycling. The enhanced stability is attributed to the formation of a robust interphase rich in borate content, which acts as a protective barrier, preventing undesirable reactions between the reactive cathode and the electrolyte. The DFT calculations reveal the mechanism and absorption energies of various decomposition products on the three surfaces of the cathode. The mechanistic study dictates that first the anion BOB^- proximity to the cathode surface loses an electron at high voltage causing B–O to break, consequently ending up in ring opening (Fig. 8a). Eventually, the unstable C_2O_4 decomposes to release CO_2 gas, while highly reactive oxalatoborate radical (1OB) attacks EC to form 1OB-EC structure resulting in boron-containing polymer structures on the surface of the cathode.[99] Interestingly the most representative 1OB-EC species generates three different negative adsorption energies on three different surfaces (Fig. 8b) by its bidentate coordination with Ni–CO, Ni–Mn, and Ni–Li, indicating that 1OB-EC polymeric structures have a tendency to get absorbed on the surface rather than dissolving into the electrolyte, thus improv-

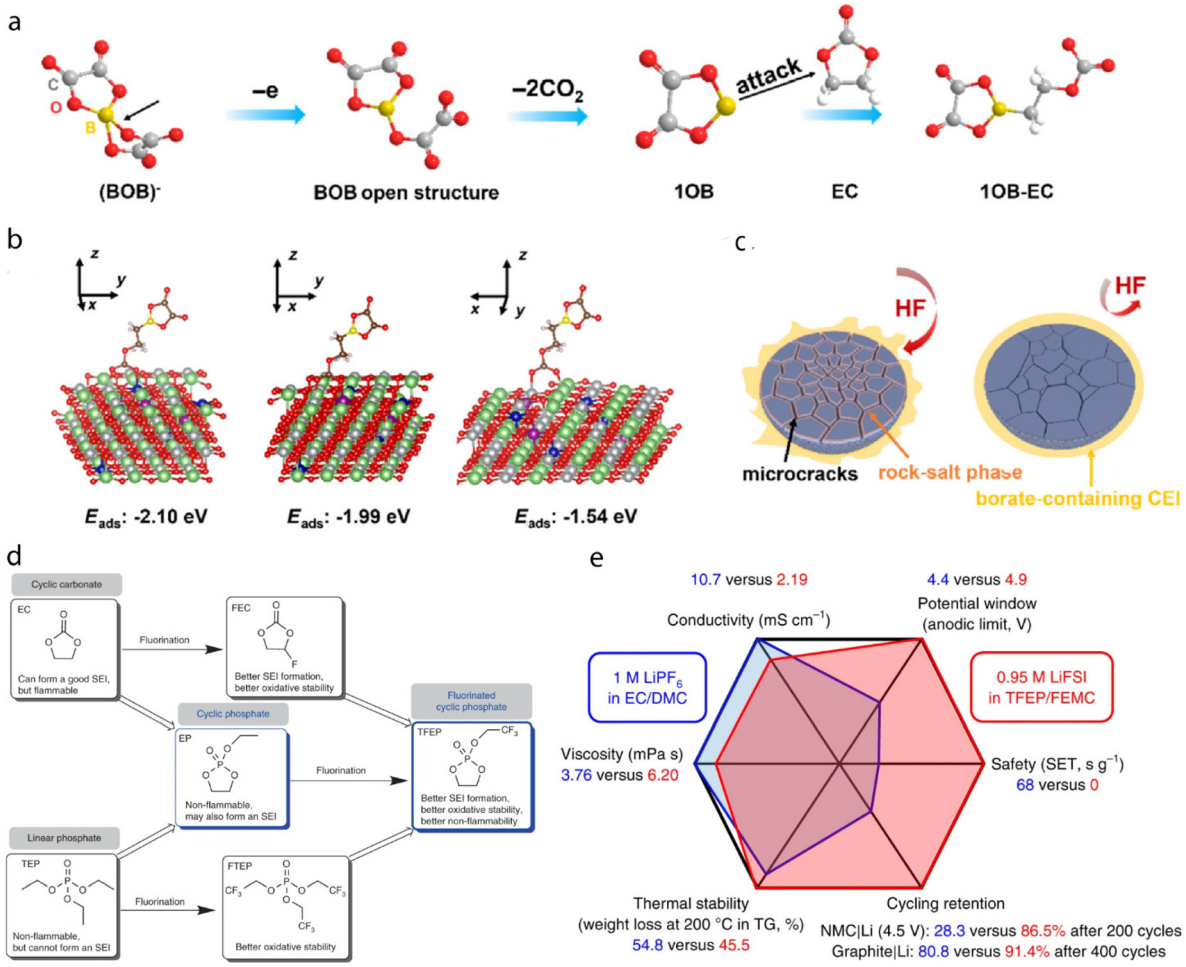

Fig. 8 (a) Schematic representation of the proposed mechanism for the decomposition of BOB^- during high voltage cycling (4.6 V). (b) Possible adsorption sites calculated using DFT. (Color code- Ni – grey; Co – blue; Mn – purple, Li – green, boron – yellow). (c) Schematic illustration of electrode morphology showing CEI of NCM83 upon cycling (left) and with 1 wt% LiBOB (right). Reproduced from ref. 100 with permission under CC 4.0. (d) Design consideration of fluorinated five-membered ring structure. (e) A comparative analysis of 0.95 M LiFSI in TEEP/FEMC against the standard 1M LiPF6 EC/DMC. Here, the axes of the hexagon signify a relative comparison of properties and performances with the superior one located at the extreme axes. Reproduced from ref. 94 with permission from Springer Nature, copyright 2020.

ing the electrochemical performances. Needless to say, more negative energy indicates the most favorable species in the reaction environments. Furthermore, the longer polymeric chains of 1OB-EC are much stronger than EC molecules and have a greater affinity to get absorbed on the surface and thus reduce the HF attacks, thus preventing microcracks and rock-salt layer formations arising from the cation mixing during cycling (Fig. 8c). Bin *et al.*[101] advocates the idea of additions of multiple additives (CsPF6, FEC, PS, TTMSPi) to improve the working window of the electrodes. The optimal performance was obtained in a wide-ranging temperature range of −40 to 60 °C while using multiple functional additives. The PC–EC ratio was optimized to extract maximum benefit and minimize the negative effect while operating in wide-ranging temperature zones. Their calculation suggests the following order $CsPF_6$ > FEC > PS > TTMSPi while following the oxidation potential and following a reverse order during reduction potential. The fundamental idea that drives the concept of multiple additives is high value of HOMO energy for one of the additives that spontaneously oxidizes to form a stable and ultrathin passivation layer on the CEI during the formation cycles. Furthermore, their high ionic conductivity additionally benefits the electrochemical performances. These additives not only participated in the CEI formation but also in the formation of the SEI on the anode side. On the anode side, these additives improved the electrode/electrolyte interphase, which improved the cycling reversibility of the Gr anode while pairing with NCA or NMC. In this race, cyclic phosphate has been proved to improve the working capability of LIB further. Using a cyclic phosphate solvent, 2-(2,2,2-trifluoroethoxy)-1,3,2-dioxaphospholane 2-oxide (TFEP), the performance of LIB can be improved significantly.[94] The design consideration is based on the idea that this molecule possesses a fused chemical structure containing cyclic carbonate which can

readily decompose to form a stable interphase, and the organic phosphate species assists in trapping hydrogen radicals and prevents combustions (Fig. 8d). Mimicking the chemical structure of EC, a five-membered ring with the non-inflammable property of phosphate and fluorinated species is synthesized. The TEEP not only assists in passivating the graphite anode, enabling long-term reversible cycles, but also assists in the formation of a stable CEI during the charged state. It is also worth mentioning here that 0.95 M LiFSI in TEEP/FEMC is stable at room temperature unless in contact with the cathode. The stable CEI formation begins with the ring-opening mechanism[102] to generate phosphate that renders nucleophilic attack on oxygen atoms to produce a metal–oxygen-rich surface. Though it may be questionable to use 0.95 M LiFSI in TEEP/FEMC against the standard 1M LiPF6 EC/DMC electrolytes, there are few striking features worth mentioning (Fig. 8e). Functional properties include wider voltage window, higher flash point, an enhanced thermal stability, a non-inflammable feature and, most importantly, long-term stability.

3.7.2 Artificial CEI and other strategies. Apart from the additive additions, the formation of an artificial CEI layer is an effective tool to promote enhanced electrochemical performances.[50] The artificial CEI offers a protective coating that helps adjust the interphase reaction and plays a dominant role in controlling lithium's charge transfer and diffusion.[103] Artificial CEI, like conventional CEI, isolates the direct contact of cathode from electrolyte, inhibits the side reactions, bestows crystal stability, and thus improves the overall electrochemical performances. During cycling, the decomposition of the electrolyte at a high cut-off potential is unavoidable, leading to the dissolution of TMs. These dissolutions generate insulating by-products such as NiF_2, CoF_2, MnF_2, which restricts the direct contact of the active particles, resulting in increased impedance and capacity decay.[105] In such a scenario, an artificial CEI can act as a protective barrier and suppress the decomposition. The introduction of Al_2O_3 can react with HF to form $PO_2F_2^-$, $Al_xO_yF_z$, and AlF_3 compounds.[103] This protective Al_2O_3 coating can act as a natural scavenger of HF and protects the material from HF corrosion and other side reactions. Recently, the Li *et al.*[103] came up with an idea of artificial CEI and introduced a robust Al_2O_3 surface layer on a thick spinel $LiNi_{0.5}Mn_{1.5}O_4$ (LNMO: high mass loading) *via* atomic layer deposition (ALD). In unmodified LNMO, the parasitic byproducts include various metal fluorides such as LiF, MnF_x, and NiF_x; however, all these species are soluble in the presence of HF, thus the cathode interphase would never be stabilized. However, in the ALD-modified LNMO, the artificially induced Al_2O_3 coating might corrode in the beginning; further corrosion is strictly restricted due to the chemical inertness of the initial generated Al–F/Al–O–F species toward HF and their water-insoluble nature (Fig. 9a). This ALD-modified LNMO improved full cell capacity retention, with the graphite anode improved from 46.3% to 75.3% (300 cycles) with cutoff voltage ~4.85 V, with appreciable CE of 99.9%. Similarly, ultrathin ALD-deposited Al_2O_3 coating is also reported to enhance the electrochemical performances of $AgVO_3$. It is also worth mentioning here that control of ALD

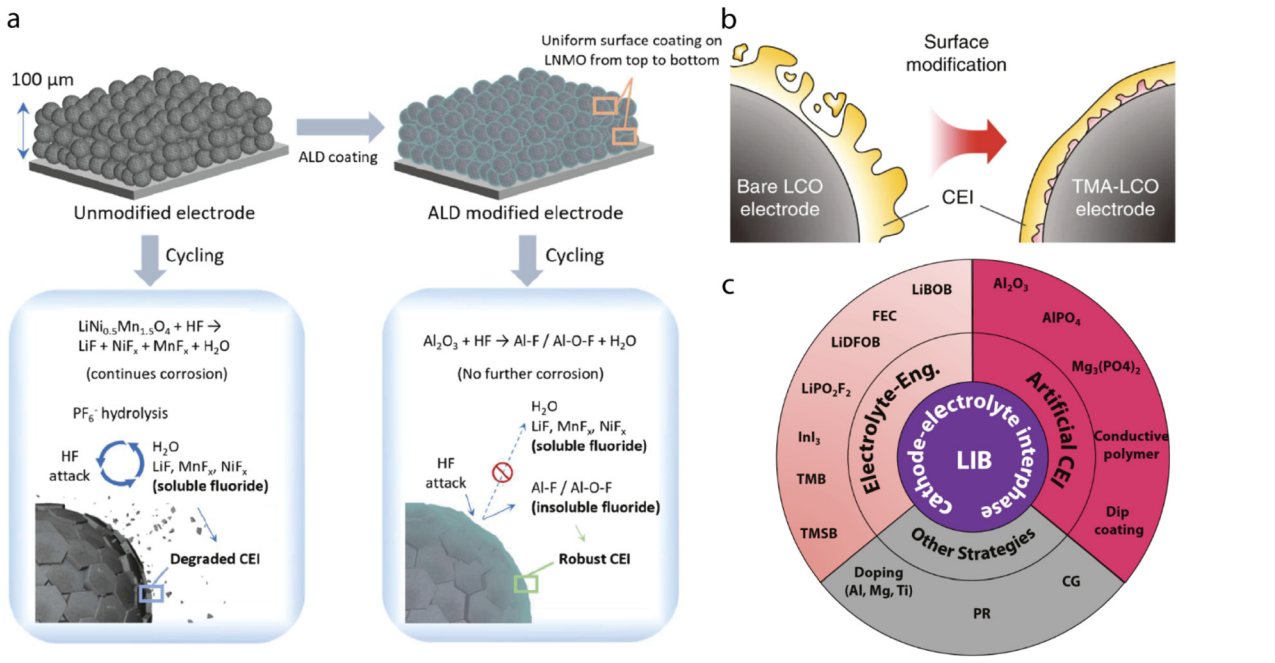

Fig. 9 (a) Schematic illustration of performance improvements in LNMO and ALD-coated LNMO. Reproduced from ref. 103 with permission from Elsevier, copyright 2022. (b) Schematic diagram showing the impact of doping to improve the CEI. Reproduced from ref. 104 with permission from Springer Nature, copyright 2018. (c) A summary of CEI improvement strategies reported so far in the literature. (Eng. – Engineering, CG – concentration gradient, PR – potentiostatic reduction).

thickness is a vital parameter to extract the maximum benefits of this coating.[106] A ~10 nm Al_2O_3 coating improved the capacity retention capability from 10% to 31% after the 100th cycle, and CE was improved from 89.8 to 98.2%. The improvements in the electrochemistry were due to suppression of vanadium dissolution into the electrolyte due to the artificial CEI, a reduction in the charge transfer resistance, and a reduced polarization voltage.

Doping is another strategy that has been widely used to stabilize the CEI. Elemental doping assists in the formation of a uniform CEI on the cathode surface.[104] Different elemental doping changes the properties of the material in different ways. Doping with Al induces a nano-island of Al_2O_3, facilitating a stable CEI and improving electrochemical performance.[107] Studies reveal that a dilute atomic-level doping of Al results in partial dissolution within the bulk. The nano-island of Al_2O_3 uniformly dresses the active particles and assists in lowering the redox potential energy of TM, consequently forming a stable CEI. Doping with Ti has the advantage of phase stabilization but promotes more Li/Ni ion exchange, which hampers the electrochemical performances in the long run. In contrast, Mg doping can enhance electronic conductivity and promote a stable CEI. As well as single dopants, trace amounts of multiple elemental doping has also reported recently, which can assist in a stable CEI and enhance electrochemical performances (Fig. 9b).[104] On the other hand, reactive ions continuously promote phase transition, thicken the CEI, and also bring irreversible impedance on the surface. Such reactive species, particularly Ni-ions, react with other species inside the cathode and continuously increase the side reactions, resulting in a decrease in CE. To restrict such side reactions, concentration gradient (CG) is a widely applied strategy in battery research.[108] Furthermore, several other strategies (Fig. 9c), in particular potentiostatic reduction (PR), an effective strategy that controls the CEI, can be used to extract optimum electrochemical performance in LIBs effectively.[109]

3.8 Some other miscellaneous factors

Though the above sections detailed the factors that influence degradation in LIBs, we now explain a few other essential factors which seriously impact electrochemical performance. Some critical aspects are gassing, thermal runaway, irreversible volume change, losing electrical/electronic contacts, and failure of binder. Of these, gassing and thermal runaway are considered as critical areas of interest particularly when batteries are operated in abusive conditions, which includes operation outside the temperature limits, overcharging, and cell deformation due to puncturing or crushing.[110–112]

Gas evolution in LIBs primarily arises from the decomposition of the electrolytes receiving a higher charging voltages at both the electrodes[113] and structural changes in the cathode.[114] Gas build-up causes swelling inside the cell; this worsens the contact between particles, which results in a sudden increase in electrical resistance; increased pressure may also lead to sudden cell failures, and the cell might eventually rupture.[115] Gas evolution due to cell component degradation is not only detrimental to electrochemical performance, it also can cause a safety risk. In this regard, a recent study revealed the impact of varying C-rates (C/20 to 4C) on the electrochemical performance of a LIB by measuring gas evolution by deploying mass spectroscopy under *operando* conditions.[115] This study, considering a commercial 1.5 A h NMC-LMO/Graphite cell, revealed that a sudden large capacity fade was noticed at high C-rates due to excessive evolution of ethylene gas. Step voltage set up between 2.6–4.2 V exhibited the release of CO_2 (>4.15 V) and H_2 at relatively lower voltages (<2.8 V). The excessive evolution of ethylene gas has been linked to the reductive decomposition mechanism of ethylene carbonate during SEI formation.[116] The plausible reason for the increasing amount of ethylene with increasing C-rate is an increased SEI build-up. This could possibly be due to rapid decomposition of the existing SEI and rebuilding of the layer, that could profusely generate more ethylene. SEI decomposition and rebuilding is one such phenomenon dependent upon temperature, which indeed increases with increases in C-rates.[117]

Before moving to discuss another factor that influences the electrochemical performances, *i.e.* thermal runaway (TR) and thermal propagation (TP), it is essential to understand a few basic facts. It is well known by now that a chemical or electrochemical reaction can become out of control on many occasions. A situation where self-heating inside the cell often becomes unstoppable gives rise to TR. This TR can cause its impact to propagate to the nearest cell pack, to sub-system or other sub-system; in the extreme they can also become out of control. This situation is called thermal runaway propagation (TRP).[118] TR and TRP are not only confined to LIB; it is a ubiquitous issue in battery technologies in general.[119,120] It is not hard to show drawbacks in the adopted definitions of TR, such as "higher heat generation than removal", and "a process of uncontrolled heat release and rapid temperature rise",[121] at least in electrochemical systems like batteries. Without giving more weight to this discussion, we would like to bring to notice that most batteries heat up during their operation, as heat generated is higher than heat removed, there is not always an uncontrolled heat release accompanying a rise in temperature, and this does not necessarily lead to dangerous levels causing damage to the cell. TR studies have become essential as there has been a rapid surge in battery demand from the electrical vehicle (EV) market, traction batteries, and future adoption in grid energy storage. Such systems have a pack of battery cells and TR, once initiated, can run through the all the cells, endangering human life and property. A recent study revealed that preventive measures, based on the assumption of venting the energized material from the battery component, could prevent cell-to-cell propagation.[122] This method relies on the idea that heat propagation in a cell is primarily through a convection process, and least by direct contact or *via* a radiative process. Real-time FTIR spectroscopy data revealed that a substantial amount of carbonate esters are removed before the TR stage is reached. These vented hot gases cool down on the top of an adjacent cell. TR could be

potentially restricted by using hybrid cooling[123] or by phase change materials (PCMs).[124] A recent study proposed a hybrid method for a thermal management system using liquid cooling and PCM.[125] In this proposed method, the operating temperature of the battery is maintained by the latent heat of PCM. During TR, PCM acts as a heat buffer and excess heat dissipates through liquid cooling to successfully avoid TR. Though this method is an effective tool to restrict the battery temperature utilizing the high thermal conductivity of PCM, it might be insufficient during TRP in extreme cases.

Another factor that needs attention is irreversible volume change. LIB cell thickness considerably changes as the cell degrades. These changes in thickness comprise reversible intercalation-induced expansion and an irreversible expansion due to TM migration to Li-sites. These changes are a strong function of temperature, depth of charge and discharge, and pressure. A study conducted under several stress factors to measure reversible and irreversible expansion revealed that a considerable reversible expansion is noticed when the cell ages compared with voltage measurements.[126] This study successfully measured voltage and expansion under several stress environments to obtain reliable and confident data for cell diagnostics in the lab. For instance, under an applied pressure, the increase in irreversible expansion is minimal compared against the applied pressure. Overall, the capacity retention and irreversible expansion is improved with increasing pressure. Strikingly, the greatest capacity fade and irreversible expansion is registered at lower pressure (1 PSI). The improvement in the electrochemical performance is primarily due to controlled/suppressed growth of the SEI at the electrode at high pressure, primarily restricting the dominant (SEI) ageing mechanism at higher temperatures. Volume change measurement inside the cell is essential to effectively deploy battery thermal management systems and curtail severe catastrophic failures. These measurements become essential as the graphite anode occupies ~35% of the total cell volume, and during charging ~10% expansion (3.35 to 3.6 Å) is registered, making it ~3.5% volume change in the cell. On the contrary, volume changes in the cathode are smaller (3.4% in NCM).[127] This differential volume expansion brings out an overall volume expansion (charge) and contraction (discharge). These repeated changes in volume over continued cycles lead to structural failure and poor electrochemical performance.[128] Irreversible volume expansion is a major source of capacity fade, and hence such volume expansions must be reduced for better operation of cell packs in LIBs. Optical volumography (OVG) is a recently developed technique to measure such volume changes.[129] This maps the strain distribution, and it also differentiates the difference between thermal-induced expansion (TIE) and reaction-induced expansion (RIE). For aged batteries, RIE becomes dominant, and it could become an essential tool to determine the state of health of the cell.

Another aspect that is often less considered is failure of binders. These small things can really make a big difference in battery performance. Capacity fading is greatly tied to the working of the binder's nature. Specifically, Si-based electrodes suffer from poor cycling due to severe mechanical stresses involved in the alloying and de-alloying process. These stresses are responsible for micro-fractures and loss of electrical contacts.[130] An electrosprayed nano-composite electrode demonstrated better capacity retention due to a two carboxymethyl cellulose binder (CMC) binding mechanism. H-bond formation between CMC and the surface of the nano-particles and the dynamic nature of this weak interaction provides a self-healing process that occurs at the sub-micron level, and the electrical contact is not lost during cycling. The battery binder (*e.g.* commonly PVDF) plays two important roles in the electrodes. Binder is an insulating material and often relies on conducting carbon to establish conducting pathways between active material and current collector. The binder experiences several mechanical stresses during the charge–discharge process. A binder is one component which experiences stress through the entire battery's lifespan. When in the dry state it experiences manufacturing stresses during calendaring to reduce porosity, and the magnitude of stress is even higher during its swelling in the battery electrolyte solvent.[131] The stresses experienced by the cathode due to repeated cycling are much higher than the yield strength of the binder, and as a result repeated cycling plastically deforms the swollen binder. This damages the binder and results in poor performance. On the other hand, binder conductivity is damaged by permanently straining the binder, which results in a conductivity difference between active material and binder. This decline in conductivity of the binder due to separated carbon particles overall decreases the conductivity of the battery.

Similarly, performance decline can also occur because of the loss of electronic contacts due to dead lithium or lithium dendrite formation at the anode surface. During oxidation, Li dendrite can lose contacts with the active material, leading to dead Li in the cell.[132] A dead Li with lost electrical contact may result in a tortuous pathway for lithium-ion transport, thereby reducing the active area for intercalation.[19] The loss of electronic contacts between electrode particles causes a sharp rise in charge transfer resistance. This loss of electrical contacts may also cause a larger hysteresis loss in the cathode, resulting in overall poor performance.[11] In a recent finding, it has been revealed that if this dead lithium can be made to move inside the cell, it will eventually touch the anode and re-establish the electrical connections by dynamically repolarizing by the application of an electric field.[133] Several studies could be undertaken to further address these issues, and it is expected that upcoming researchers will take up these challenges in their future work.

Before moving to other discussions, quantifying the contributions from each factor that influences the battery degradation could be essential. However, an exact % contribution could be hard to find, as many of the factors often interplay among each other, making the analysis very complex. Nonetheless, digging out from the literature, it is established that the TR contribution in an individual Li-ion cell is low, one in tens-of-millions.[122] But this may rise with the number of cells in a battery as well as number of batteries deployed

worldwide in the near future. The majority of failures in batteries are temperature dependent. Thus, it could be said that a relatively larger contribution toward degradation comes from temperature. Low and high temperature both impact the cell performance severely. Working under lower temperature causes confined spaces for lithium intercalation, thereby causing lithium plating and subsequent capacity fading. While operating under high temperature (40–60 °C) brings more capacity, it also brings a rapid cell degradation rate.[7]

Though an exact estimation is challenging to obtain, more precise data could be obtained by statistical analysis, which involves collecting data from the literature on battery degradation, including factors such as charge-depth, temperature, and cycle number, and so on. Machine learning is another handy tool that could be used to develop algorithms considering several degradation factors. These algorithms could be helpful to quantify the contribution from each factor. Similarly, experimental testing can be performed additionally to verify the findings from the two approaches mentioned above.

4. Techniques to investigate the degradation

Understanding the degradation mechanism is crucial for designing better electrode materials for advanced-generation batteries. Thus, dedicated efforts must be made to understand the origin of degradation in contemporary battery materials explicitly. There are several electrochemical tools for understanding electrochemical performance, such as electrochemical impedance spectroscopy (EIS), a core technique to decouple resistance contributions, open circuit voltage (OCV) itself used to calculate the state of charge (SoC), and differential voltage analysis.[134] In addition, a range of spectroscopy techniques is essential to monitor physical and chemical changes in the electrode itself. Spectroscopic techniques such as *in situ*, *ex situ*, and *operando* techniques are straightforward for visualization of the origin of degradation and its impact on battery components.

4.1 Electrochemical techniques

Electrochemical techniques are commonly used to investigate the degradation of lithium-ion batteries. These techniques involve measuring the battery's electrochemical performance, such as capacity, internal resistance, and charge–discharge efficiency. By monitoring these parameters over time, researchers can identify changes in the battery's performance indicative of degradation. Various techniques, including cyclic voltammetry, electrochemical impedance spectroscopy, potentiostatic intermittent titration technique (PITT), and charge–discharge cycling, are used to monitor the degradations in batteries. In recent research, researchers have been able to unlock the long-standing issues in LIBs pertaining to their irreversible first-cycle capacity loss.[135] In some materials, this irreversible first-cycle capacity loss can be as high as >60 mA h g^{-1}. Though we do not explain a number of theories and experiments conducted earlier to explain this capacity loss, in summary, irreversible oxygen release is partly blamed for this capacity loss in cathodes.[136] A typical first-cycle charge–discharge with high cut-off voltage (4.8 V) and capacity loss is shown in Fig. 10a. The charging cycle can be divided into two regions containing a sloped zone followed by a plateau ~4.5 reflecting the oxidations of TMs (Ni^{2+}, Co^{3+}) and O^{2-}, respectively. The subsequent discharge follows a conventional S-shaped profile. To exactly pinpoint at which point irreversible capacity originates, predetermined charge capacities from 5–400 mA h g^{-1} were measured (Fig. 10b). Several studies revealed that irreversible capacities in the first cycle could be recovered by deep discharge down to lower potential.[137] To justify this idea, the authors measured a low discharge (1.0 V), and some exciting results were obtained. To further reveal the kinetic mechanism of irreversible capacity at low voltage, a comprehensive analysis of time-scaled galvanostatic intermittent titration technique (GITT) analysis was conducted (Fig. 10c). The voltage plateau above 3.0 V represents the lithiated Li_xMO_2 phase, while the voltage plateau around 1.5 V corresponds to the Li_2MO_2 phase. From the figure, it can be noted that the overpotential between both phases is <0.4 V. However, there are two regions (yellow and green color) exhibiting a potential gap >1 V between the kinetic–thermodynamic state. The yellow color marks a gradual drop in kinetic-potential while its thermodynamic potential is stable. This is particularly due to the slow Li-diffusion. The green region depicts a decline in thermodynamic-state potential while the kinetic-state-potential remains reasonably stable. Interestingly, the Li-ion diffusion coefficient is even higher than $LiMO_2$ phase above 3.5 V. It so happens that the first-cycle irreversible capacity is dominated by kinetic-related irreversible capacities when less than ~3/4 of Li is extracted from the Li_2MnO_3, while oxygen-related irreversible capacity loss is reported when more than 3/4 of Li is extracted from the Li_2MnO_3 phase precisely when x = 0.2 in $Li_xNi_{0.13}Co_{0.13}Mn_{0.54}O_2$ (Fig. 10d). This finding highlights that unrecoverable O_2 release in Li-excess cathode structures is triggered when $x < 0.2$ in $Li_xNi_{0.13}Co_{0.13}Mn_{0.54}O_2$.

4.2 Microscopy techniques

Microscopy techniques, such as atomic force microscopy (AFM), scanning electron microscopy (SEM), and transmission electron microscopy (TEM), are widely used to investigate the structural degradation of LIBs. These techniques allow researchers to observe changes in the morphology of the electrodes and the formation of solid–electrolyte interphase (SEI) layers. SEM and TEM can also be used to identify the presence of lithium dendrites, which can cause short circuits and lead to battery failure. A dendritic formation is a common form of battery degradation, especially in LIBs.[138] Dendrites are tiny, needle-like structures that grow from the surface of the negative electrode and penetrate through the electrolyte to the positive electrode. These dendrites can cause short circuits and reduce the performance and safety of the battery. Several

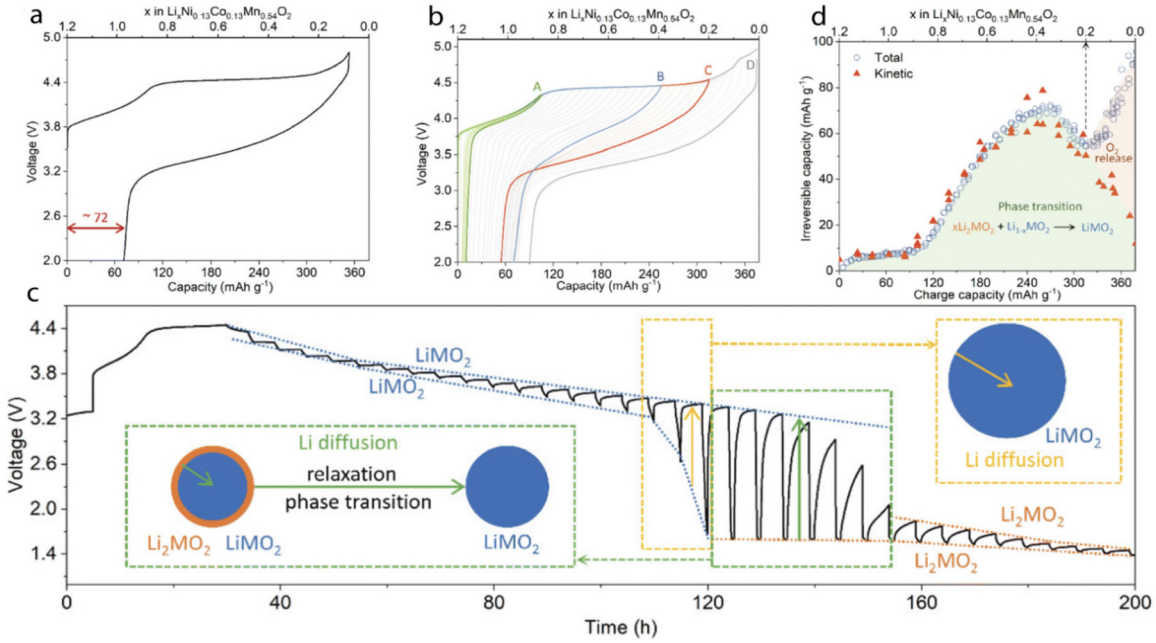

Fig. 10 (a) Depicting the first cycle irreversible capacity loss in $Li_{1.2}Ni_{0.13}Co_{0.13}Mn_{0.54}O_2$. (b) Controlled charged-discharge profile for the first cycle from 5–400 mA h g^{-1}. (c) Time-scaled GITT profile for $Li_xNi_{0.13}Co_{0.13}Mn_{0.54}O_2$. (d) Representation decomposition in $Li_xNi_{0.13}Co_{0.13}Mn_{0.54}O_2$ reflecting the first cycle irreversible capacity loss. Reproduced from ref. 135 with permission from the RSC, copyright 2023.

factors can contribute to dendrite formation, including the use of low-quality materials, high current density, and overcharging. Temperature fluctuations, mechanical stress, and electrolyte composition can also exacerbate the growth of dendrites. To mitigate dendrite formation, researchers are exploring various approaches, including using additives in the electrolyte, solid-state electrolytes, and developing new electrode materials more resistant to dendrite growth. In addition to dendrite formation, other forms of degradation can occur in batteries, such as capacity loss, internal short circuits, and electrode corrosion. These degradation mechanisms can also be investigated using microscopy techniques. Understanding and mitigating these forms of degradation is crucial for improving batteries' performance, safety, and lifespan. Recently, it has been found that engineering stresses inside the battery can largely suppress the dendrite formations.[139] In this study, the authors hypothesized the idea of applying mechanical loads to growing dendrites in $Li_{6.6}La_3Zr_{1.6}Ta_{0.4}O_{12}$ (LLZTO) solid electrolytes. The use of *operando* microscopy revealed a noticeable change in the trajectory of dendrite growth when compressive loading was initiated, ultimately preventing cell failure (Fig. 11). Through the application of fracture mechanics, the impact of stack pressure and in-plane stresses on dendrite trajectory was quantified, and the residual stresses necessary to prevent short-circuit failure were charted. Design approaches for achieving such stresses were also proposed. This study has shown that metal dendrite responses are correlated to applied mechanical loads, as evidenced by Fig. 11. Specifically, Fig. 11a displays the results for a 90 μm-thick LLZTO electrolyte disk, where a dendrite was allowed to propagate under 0.2 mA cm^{-2} current density and was subjected to 70 MPa of applied compression, followed by unloading. The blue highlighting shows the dendrite's path under no applied load, while the red highlights the segment propagating under load. Their findings indicate that the dendrite deflects towards the loading axis when loaded and returns to its original propagation direction when unloaded. The tendency for dendrites to align with the applied load is similar to the propagation of a pressurized crack. The pressure buildup within the metal protrusion due to continuous metal plating results in pressure on the flaw surface. Thus, under increased load, cracks tend to turn towards the compression axis, consistent with the experimental results presented in Fig. 11a. The response of the metal dendrite formation along the horizontal direction was also calculated, as shown in Fig. 11b. Following the application of a load, it was observed that the dendrites display a kink towards the stripping electrode, which is in the direction of compression. The authors also designed a mathematical model to understand the dendrite trajectory under mechanical loading (Fig. 11c–g). This model represents dendrites as metal-filled flaws with a slit-like shape, oriented at an initial angle to the horizontal plane, as shown in Fig. 11c. The electrolyte/electrode interface is held with fixed horizontal displacement in a homogeneous and isotropic solid electrolyte. It was assumed that plating metal into the flaw generates a uniform pressure normal to the flaw face, causing the dendrite to propagate forward without any kinking in the absence of other stresses in the electrolyte. However, when an additional load (σ_{yy}) is applied to the solid electrolyte in the vertical direction, the preferred path for dendrite propagation becomes

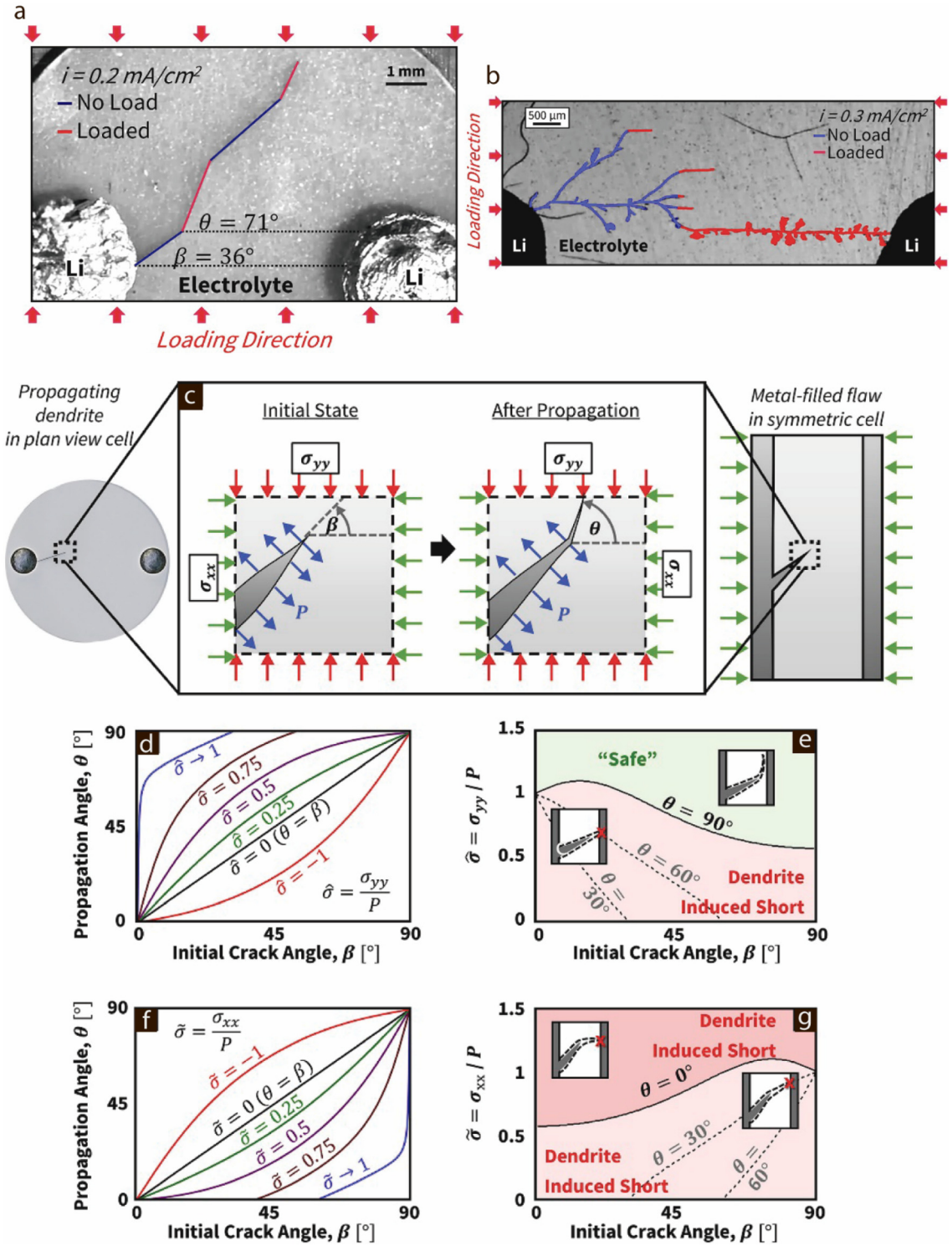

Fig. 11 (a) Image showing the response of a metal dendrite to electrochemical and mechanical loadings in LLZTO. (b) A response along the horizontal direction. A response upon mixed mode fracture: (c) propagating dendrite in a plan view cell, (d) response along the most favorable propagation angle against initial crack angle β, (e) different values of $\hat{\sigma}$ to produce various angles against initial crack angle β, (f) energetically favorable propagation angle θ as a function of inclination angle β for $\hat{\sigma} = \sigma_{xx}/P$, (g) plots of $\hat{\sigma}$ against β. Reproduced from ref. 139 with permission from Elsevier, copyright 2022.

kinked at an angle from its initial orientation, as seen in Fig. 11c. The stress state in front of the crack tip results from the superposition of the plating-induced pressure and the applied load, and the preferred propagation angle (Fig. 11c) maximizes the local mode I stress intensity factor for an infinitesimal extension of the crack tip. The optimal angle for den-

drite propagation as a function of the initial crack inclination angle β and different values of $\hat{\sigma} = \sigma_{xx}/P$ is shown in Fig. 11d. The black curve represents the case where the only stress in the system is P, (*i.e.*, $\hat{\sigma} = 0$), resulting in $\theta = \beta$. As values become more positive ($\hat{\sigma}$), indicating higher compressive loads, θ increases relative to that for $\hat{\sigma} = 0$, causing deflection. The series labeled $\hat{\sigma}1$ presents the solution for θ as $\hat{\sigma}$ approaches 1. When θ reaches 90°, the dendrite cannot reach the counter-electrode, regardless of the electrolyte's lateral dimensions. The results indicate that P is approximately equal to the fracture stress of the electrolyte. The other values of $\hat{\sigma}$ required to produce θ = 90°/60°/30° as a function of β are shown in Fig. 11e. Some other energetically favorable θ values as a function of β for different values of $\hat{\sigma} = \sigma_{xx}/P$ are shown in Fig. 11f. In addition, a few other r values of $\hat{\sigma}$ required to produce θ = 0°/30°/60° as a function of β are shown in Fig. 11g. The study concluded that electrolyte fracture dictates dendrite propagation, with electronic leakage playing a negligible role in the process for the studied materials. While such fundamental studies are essential, it is also crucial that further experimental studies are carried out to confirm the validity of such models.

4.3 Spectroscopy techniques

Spectroscopy techniques, such as Fourier transform infrared spectroscopy (FTIR) and X-ray photoelectron spectroscopy (XPS), are commonly used to investigate the chemical degradation of LIBs. FTIR can be used to identify changes in the composition of the SEI layer, while XPS can be used to identify changes in the chemical composition of the electrodes. Nowadays, fast-charging batteries are urgently required for fast-paced electrified societies. Thus to realize fast charging of LIBs and facilitate electric vehicle adoption, it is necessary to investigate ion transport and develop appropriate electrolytes. FTIR with attenuated total reflection (ATR) is useful for conducting *operando* measurements of liquid electrolytes. A recent study focused on solvation shifting of solvent infrared absorption bands in the presence of lithium ions, comparing lithium-shifted and non-shifted bands of ethyl methyl carbonate (EMC) and ethylene carbonate (EC) to infer changes in ion concentration during cycling.[140] Lithium concentrations were calibrated using EC/EMC/$LiPF_6$ electrolytes with known concentrations. A Li-ion half-cell with a graphite anode and EC/EMC/$LiPF_6$ electrolyte was examined using FTIR/ATR. The study revealed that the magnitude of lithium concentration changes increased with a higher C-rate, and changes in lithium concentration could be observed during a GITT test. A negative current caused lithium depletion during intercalation, whereas a positive current caused a lithium surplus during deintercalation. Observing lithium concentration has significant implications for *operando* studies and linking lithium movement to battery performance.

4.4 Thermal analysis techniques

Thermal analysis techniques, for instance, differential scanning calorimetry (DSC) and thermal gravimetric analysis (TGA), can be used to investigate the thermal degradation of lithium-ion batteries. DSC can be used to measure the heat released during thermal runaway events, while TGA can be used to measure changes in the mass of the battery components during heating. A recent report uses an accelerating rate calorimeter (ARC) to study the thermal runaway of commercial lithium-ion cells based on different cathode materials: $LiCoO_2$ (LCO), $LiFePO_4$ (LFP), and $LiNi_xCo_yAl_{1-x-y}O_2$ (NCA), at various states of charge (SOC).[141] The study includes the evaluation of the individual component properties of the cells by using TGA, DSC, and temperature-resolved X-ray diffraction (TR-XRD). The results indicate that the onset of thermal runaway decreases and peak heating rate increases with increasing SOC due to cathode destabilization. The LCO and NCA cathodes are metastable and exhibit higher thermal runaway rates compared with the LFP cathode, which is stable even when charged at high temperatures. The decomposition and self-heating onset temperature of the anodes are generally independent of SOC, whereas the onset temperatures of the cathodes are typically observed above the onset of whole cell runaway in the ARC. This study provides a scientific basis for future thermal modeling and design of safer lithium-ion cells. By correlating the contribution of individual cell components to thermal runaway trends, this study emphasizes the need to consider the material aspects of lithium-ion battery design to ensure safety during use. One of the studies on dual-salt electrolytes using bis(trifluoromethanesulfonyl)imide (LiTFSI) and lithium difluoro(oxalato)borate (LiODFB) in carbonate solvents for LIB gave a few interesting results under ARC and DSC study.[142] The LiTFSI–LiODFB dual salt decomposes at a temperature of 138.5 and 271.0 °C, in DSC and ARC tests, respectively. The former is the onset decomposition temperature of the solvent, while the latter is the LiTFSI–LiODFB dual salt. Applying various mathematical models (discussed in the next section), it was found that the activation energy for the dual salt (53.25 kJ mol^{-1}) was much better than the commercial/conventional $LiPF_6$ electrolytes in terms of stability. As soon as the temperature rises above 89.3 °C, $LiPF_6$ electrolytes experience an endothermic reaction generating a strong Lewis acid (LiF, PF_5) and further accelerating the decomposition reaction rate. When the temperature rises, strong Lewis acid PF_5 promotes ring opening polymerization reactions and accelerates the decompositions of $LIPF_6$ and the other organic volatile solvents. This situation then becomes a matter of serious concern toward the thermal safety of the batteries, and often results in thermal runaway and catastrophic failure, which by any means must be stopped.

4.5 Mathematical modeling

Mathematical modeling is a powerful tool for investigating the degradation mechanisms of lithium-ion batteries. Models can be used to simulate the electrochemical, structural, and chemical changes that occur during charge and discharge cycles. Researchers can gain insight into the underlying mechanisms contributing to battery degradation by comparing model predictions with experimental data. There are several

approaches for modeling battery degradation, but one common method is to use empirical models. These models are constructed on experimental data obtained from actual battery cycling tests. The data are used to develop a mathematical equation that describes how the battery's performance changes over time. One widely used empirical model is the "capacity fade" model, which describes how the battery's capacity (*i.e.*, its ability to store energy) decreases over time as it undergoes charging and discharging cycles. The capacity fade model is typically expressed as a simple mathematical equation, such as $C(t) = C\_0 \times \exp(-kt)$, where $C(t)$ is the battery capacity at time t, C_0 is the initial capacity of the battery, k is a rate constant that describes the rate of capacity loss, and exp is the exponential function. Other models can describe other types of battery degradation, such as changes in internal resistance or changes in the battery's chemical composition. These models typically involve more complex mathematical equations and may require more experimental data to develop. Mathematical modeling can be a valuable tool for understanding and predicting battery degradation, which is essential for designing more efficient and reliable battery systems.

Battery life prediction has been a significant subject of investigation since the implementation of EVs. Over time, several models have been predicted by various groups.[144,145] However, in general, it can be summarized as shown in Fig. 12. The electrochemical model can be obtained considering physics-based modeling, requiring moderate data, and can be, to an extent, computed on physical and chemical laws (Fig. 12a). Modeling based on a semi-empirical model (Fig. 12b) is used when performance-based modeling is required. This model requires extensive data to predict the data efficiently. With the inception of artificial intelligence (AI), mathematical modeling for predicting battery life has gained a boost. Though these models require extensive training set data (sometimes called the data-driven models), they promise to give accurate data close to a real-world scenario. Data-driven battery models are mathematical models developed using data from real-world battery systems (Fig. 12c). These models could be used to predict the behavior of batteries under different operating conditions and to optimize battery performance. Various types of data-driven battery models exist, including empirical, black-box, and grey-box models. Empirical models are the simplest type of data-driven models based solely on experimental data. They are often used to estimate the SoC, and are sometimes also referred to as state of health (SoH) of a battery and its performance characteristics. Black-box models are more complex than empirical models, and are often used when the underlying physics of the battery is not well understood or too complex to model. Black-box models use statistical techniques, such as machine learning (ML) algorithms, to learn the relationship between input and output variables from the data. Grey-box models combine

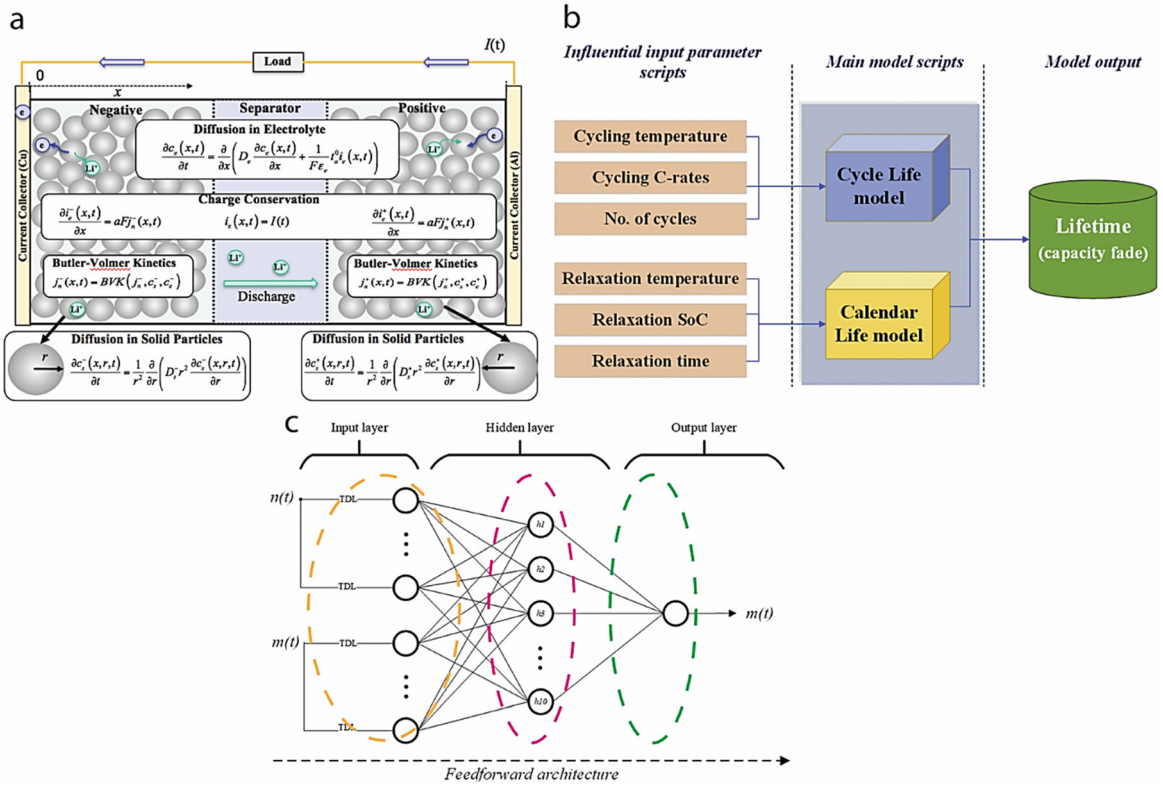

Fig. 12 Various battery modeling approaches at a glance. (a) Electrochemical modeling. (b) Semi-empirical modeling. (c) Data-driven model. Reproduced from ref. 143 with permission from Elsevier, copyright 2021.

aspects of both empirical and black-box models. They incorporate some of the known physics of the battery into the model while also using experimental data to refine the model parameters.

Battery modeling is an important area of research because it can help to optimize battery performance, reduce costs, and extend the life of batteries. Battery models are used in a wide range of applications, including EVs, renewable energy systems, and portable electronic devices.

5. Summary and outlook

Developing high-performance batteries that meet the requirements for various applications needs a thorough understanding of battery degradation. This review has identified primary degradation mechanisms responsible for battery degradation during normal operation, including SEI layer growth, CEI, lithium plating, and particle fracture at both electrodes. At the cell level, all of these degradation mechanisms result in loss of lithium inventory, loss of active material at both electrodes, impedance change, and stoichiometric drift, ultimately leading to performance degradations such as capacity or voltage fade. It is important to note that calendar or cycle aging represent different pathways through the degradation space characterized by these mechanisms. It is to be mentioned here that there is no universally accepted degradation mechanism, and several other mechanisms must be explored with the inception of novel materials. Furthermore, these degradation mechanisms may couple with other mechanisms, making the situation even more complex. Thus extensive studies are required to understand the degradation mechanisms in the batteries thoroughly.

Before battery models can be applied accurately to specific chemistries, applications, or stages of battery life, they must first be parameterized. There are several experimental and atomistic techniques available for parameterizing batteries, but these methods are not well understood. As a result, there is a need for a coordinated effort to review and standardize battery parameterization techniques.

In summary, this review presents the most recent updates on understanding battery degradation in LIBs. However, a few advanced cathode materials such as high entropy cathodes, partial spinels, and partially disordered cathodes, are not explored here due to the unavailability of much research data, as these materials are very new. We strongly encourage and suggest that future battery researchers take up the challenges of these materials and understand their degradation pathways to synthesize them with a better prospect when they are used in future EVs.

Conflicts of interest

There are no conflicts to declare.

Acknowledgements

This work was supported by the National Research Foundation of Korea (NRF) grant funded by the Korean government (MSIP) (NRF-2022R1A2C2009459) and the Korea Institute of Energy Technology Evaluation and Planning (KETEP) and the Ministry of Trade, Industry & Energy (MOTIE) of the Republic of Korea (No. 20224000000020).

References

1 A. Manthiram, *Nat. Commun.*, 2020, **11**(1), 1550.
2 *Angew. Chem., Int. Ed.*, 2019, **58**(47), 16723.
3 J. B. Goodenough and K.-S. Park, *J. Am. Chem. Soc.*, 2013, **135**(4), 1167.
4 A. N. Singh, *et al.*, *Small*, 2021, **17**(18), 2005605.
5 M. Kabir and D. E. Demirocak, *Int. J. Energy Res.*, 2017, **41**(14), 1963.
6 J. Zhu, *et al.*, *Cell Rep. Phys. Sci.*, 2021, **2**(8), 100537.
7 M. M. Kabir and D. E. Demirocak, *Int. J. Energy Res.*, 2017, **41**(14), 1963.
8 S. N. S. Hapuarachchi, *et al.*, *Adv. Sustainable. Syst.*, 2018, **2**(8–9), 1700182.
9 T. Liu, *et al.*, *Nature*, 2022, **606**(7913), 305.
10 A. N. Singh, *et al.*, *Matter*, 2022, **5**(9), 2587.
11 J. P. Pender, *et al.*, *ACS Nano*, 2020, **14**(2), 1243.
12 A. N. Singh, *Matter*, 2021, **4**(1), 23.
13 K.-J. Park, *et al.*, *ACS Energy Lett*, 2019, **4**(6), 1394.
14 J. Zhu, *et al.*, *J. Power Sources*, 2020, **448**, 227575.
15 J. S. Edge, *et al.*, *Phys. Chem. Chem. Phys.*, 2021, **23**(14), 8200.
16 C. R. Birkl, *et al.*, *J. Power Sources*, 2017, **341**, 373.
17 J. M. Reniers, *et al.*, *J. Electrochem. Soc.*, 2019, **166**(14), A3189.
18 X.-G. Yang, *et al.*, *J. Power Sources*, 2017, **360**, 28.
19 X. Lin, *et al.*, *Prog. Energy Combust. Sci.*, 2021, **87**, 100953.
20 A. Mauger, *et al.*, *J. Electrochem. Soc.*, 2020, **167**(7), 070507.
21 J. Du, *et al.*, *Batteries*, 2022, **9**(1), 3.
22 A. Wang, *et al.*, *npj Comput. Mater.*, 2018, **4**(1), 15.
23 J. Kim, *et al.*, *J. Electrochem. Soc.*, 2021, **168**(3), 030521.
24 Q. Wang, *et al.*, *Prog. Energy Combust. Sci.*, 2019, **73**, 95.
25 S. K. Heiskanen, *et al.*, *Joule*, 2019, **3**(10), 2322.
26 J. D. McBrayer, *et al.*, *Nanotechnology*, 2021, **32**(50), 502005.
27 P. Yan, *et al.*, *Nat. Commun.*, 2017, **8**(1), 14101.
28 H. J. Ploehn, *et al.*, *J. Electrochem. Soc.*, 2004, **151**(3), A456.
29 M. Safari, *et al.*, *J. Electrochem. Soc.*, 2009, **156**(3), A145.
30 U. S. Vogl, *et al.*, *J. Electrochem. Soc.*, 2015, **162**(4), A603.
31 X. M. Xu, *et al.*, *AIP Adv.*, 2018, **8**(10), 105323.
32 Z. Ruff, *et al.*, *J. Electrochem. Soc.*, 2021, **168**(6), 060518.
33 Y. K. Lee, *J. Power Sources*, 2021, **484**, 229270.
34 E. Peled, *J. Electrochem. Soc.*, 1979, **126**(12), 2047.
35 M. G. S. R. Thomas, *et al.*, *J. Electrochem. Soc.*, 1985, **132**(7), 1521.
36 N. Zhang, *et al.*, *Cell Rep. Phys. Sci.*, 2022, **3**(12), 101197.

37 D. Aurbach, *J. Power Sources*, 2000, **89**(2), 206.
38 Y. S. Jung, *et al.*, *Adv. Energy Mater.*, 2013, **3**(2), 213.
39 J.-N. Zhang, *et al.*, *Energy Storage Mater.*, 2018, **14**, 1.
40 S. Fang, *et al.*, *J. Power Sources*, 2018, **373**, 184.
41 X. Yu, *et al.*, *Adv. Energy Mater.*, 2014, **4**(5), 1300950.
42 W. Li, *et al.*, *Nat. Commun.*, 2017, **8**(1), 14589.
43 J. Alvarado, *et al.*, *Mater. Today*, 2018, **21**(4), 341.
44 X. Zhang, *et al.*, *Mater. Today*, 2021, **44**, 15.
45 X. Zhang, *et al.*, *Adv. Energy Mater.*, 2020, **10**(22), 2000368.
46 X. Ren, *et al.*, *Joule*, 2019, **3**(7), 1662.
47 Y. Wu, *et al.*, *Energy Storage Mater.*, 2021, **37**, 77.
48 S. Chen, *et al.*, *Joule*, 2019, **3**(4), 1094.
49 Y. Cao, *et al.*, *Nat. Nanotechnol.*, 2019, **14**(3), 200.
50 T. Kim, *et al.*, *J. Mater. Chem. A*, 2023, **11**(1), 221.
51 X. Yu, *et al.*, *Adv. Energy Mater.*, 2014, **4**(5), 1300950.
52 C. Liu, *et al.*, *Mater. Today*, 2016, **19**(2), 109.
53 J. C. Garcia and T. D. Burleigh, *Electrochem. Soc. Interface*, 2013, **22**(2), 36.
54 L. B. Hunt, *Gold Bull.*, 1973, **6**(1), 16.
55 T. Waldmann, *et al.*, *J. Power Sources*, 2018, **384**, 107.
56 N. Kanani, *Electroplating: basic principles, processes and practice*, Elsevier, 2004.
57 D. Ren, *et al.*, *eTransportation*, 2019, **2**, 100034.
58 M. Avdeev, *et al.*, *Appl. Surf. Sci.*, 2017, **424**, 378.
59 C. von Lüders, *et al.*, *J. Power Sources*, 2017, **342**, 17.
60 Q. Liu, *et al.*, *J. Electrochem. Soc.*, 2017, **164**(6), A1173.
61 V. Zinth, *et al.*, *J. Power Sources*, 2014, **271**, 152.
62 A. Iturrondobeitia, *et al.*, *J. Phys. Chem. C*, 2017, **121**(40), 21865.
63 B. P. Matadi, *et al.*, *J. Electrochem. Soc.*, 2017, **164**(6), A1089.
64 Y. Xie, *et al.*, *J. Power Sources*, 2022, **542**, 231753.
65 H.-J. Kim, *et al.*, *ACS Appl. Mater. Interfaces*, 2020, **12**(9), 10268.
66 A. N. Singh, *et al.*, *Nanomaterials*, 2023, **13**(5), 905.
67 A. N. Singh, *et al.*, *Nanomaterials*, 2023, **13**(1), 10.
68 A. M. Abeysekera, *et al.*, *Chem. Commun.*, 2022, **58**(68), 9480.
69 A. N. Singh, *et al.*, *Adv. Energy Mater.*, 2020, **10**(30), 2000768.
70 I. Takahashi, *et al.*, *ACS Appl. Energy Mater.*, 2019, **2**(11), 8118.
71 A. N. Singh and K.-W. Nam, *Matter*, 2022, **5**(5), 1347.
72 G.-L. Xu, *et al.*, *Nat. Commun.*, 2022, **13**(1), 436.
73 M. Jiang, *et al.*, *Adv. Energy Mater.*, 2021, **11**(48), 2103005.
74 G. Li, *et al.*, *J. Solid State Electrochem.*, 2017, **21**(3), 673.
75 S. Ma, *et al.*, *Prog. Nat. Sci.: Mater. Int.*, 2018, **28**(6), 653.
76 J. Li, *et al.*, *Appl. Energy*, 2018, **212**, 1178.
77 S. E. J. O'Kane, *et al.*, *Phys. Chem. Chem. Phys.*, 2022, **24**(13), 7909.
78 F. P. McGrogan, *et al.*, *J. Electrochem. Soc.*, 2017, **164**(14), A3709.
79 D. Huang, *et al.*, *ACS Appl. Mater. Interfaces*, 2021, **13**(10), 11930.
80 W. Li, *et al.*, *Chem. Soc. Rev.*, 2017, **46**(10), 3006.
81 B. L. D. Rinkel, *et al.*, *Energy Environ. Sci.*, 2022, **15**(8), 3416.
82 S. Nikman, *et al.*, *Electrochim. Acta*, 2021, **386**, 138373.
83 W. B. Hawley, *et al.*, *J. Power Sources*, 2020, **466**, 228315.
84 J. Qian, *et al.*, *Nat. Commun.*, 2018, **9**(1), 4918.
85 R. J. Gummow, *et al.*, *Solid State Ionics*, 1994, **69**(1), 59.
86 W. Lu, *et al.*, *ACS Appl. Mater. Interfaces*, 2017, **9**(22), 19313.
87 Y. Chen, *et al.*, *Adv. Energy Mater.*, 2022, **12**(33), 2201631.
88 W. M. Dose, *et al.*, *ACS Appl. Mater. Interfaces*, 2022, **14**(11), 13206.
89 T. Yoon, *et al.*, *J. Power Sources*, 2021, **503**, 230051.
90 F. Wu, *et al.*, *Energy Storage Mater.*, 2021, **41**, 495.
91 K. Dai, *et al.*, *Adv. Funct. Mater.*, 2021, **31**(13), 2008632.
92 F. Liu, *et al.*, *Chem. Eng. J.*, 2022, **434**, 134745.
93 S. Ge, *et al.*, *Sci. Adv.*, 2020, **6**(9), eaay7633.
94 Q. Zheng, *et al.*, *Nat. Energy*, 2020, **5**(4), 291.
95 Y. Zheng, *et al.*, *ACS Appl. Energy Mater.*, 2020, **3**(3), 2837.
96 Q. Liu, *et al.*, *ACS Appl. Mater. Interfaces*, 2019, **11**(19), 17435.
97 Y.-Q. Chen, *et al.*, *J. Power Sources*, 2020, **477**, 228473.
98 W. Zhao, *et al.*, *Adv. Energy Mater.*, 2018, **8**(19), 1800297.
99 Z. Xiao, *et al.*, *Mater. Chem. Front.*, 2020, **4**(6), 1689.
100 F. Wu, *et al.*, *InfoMat*, 2023, **5**(8), e12462.
101 B. Liu, *et al.*, *ACS Appl. Mater. Interfaces*, 2019, **11**(24), 21496.
102 N. von Aspern, *et al.*, *ACS Appl. Mater. Interfaces*, 2019, **11**(18), 16605.
103 W. Li, *et al.*, *Energy Storage Mater.*, 2022, **49**, 77.
104 J.-N. Zhang, *et al.*, *Nat. Energy*, 2019, **4**(7), 594.
105 A. Fu, *et al.*, *Energy Storage Mater.*, 2022, **46**, 406.
106 L. Liu, *et al.*, *Nanomaterials*, 2021, **11**(3), 569.
107 L. Zou, *et al.*, *Nat. Commun.*, 2019, **10**(1), 3447.
108 J. Jeyakumar, *et al.*, *J. Colloid Interface Sci.*, 2023, **639**, 145.
109 P. Bai, *et al.*, *Angew. Chem., Int. Ed.*, 2022, **61**(26), e202202731.
110 B. Rowden and N. Garcia-Araez, *Energy Rep.*, 2020, **6**, 10.
111 S. Shahid and M. Agelin-Chaab, *Energy Convers. Manage.: X*, 2022, **16**, 100310.
112 T. Amalesh and N. L. Narasimhan, *J. Power Sources*, 2020, **479**, 228775.
113 M. Leißing, *et al.*, *Batteries Supercaps*, 2021, **4**(11), 1731.
114 H. Q. Pham, *et al.*, *J. Power Sources*, 2022, **527**, 231181.
115 U. Mattinen, *et al.*, *J. Power Sources*, 2020, **477**, 228968.
116 S. Solchenbach, *et al.*, *J. Electrochem. Soc.*, 2018, **165**(14), A3304.
117 K. Kleiner and H. Ehrenberg, *Electrochemical Energy Storage: Next Generation Battery Concepts*, 2019, p. 169.
118 A. Börger, *et al.*, *J. Energy Storage*, 2019, **24**, 100649.
119 A. N. Singh, *et al.*, *Adv. Funct. Mater.*, 2023, 2304617.
120 S. Mallick and D. Gayen, *J. Energy Storage*, 2023, **62**, 106894.
121 B. Barnett, *et al.*, *Lithium-Ion Batteries, Safety*, in *Batteries for Sustainability: Selected Entries from the Encyclopedia of Sustainability Science and Technology*, ed. R. J. Brodd, Springer New York, New York, NY, 2013, p. 285.

122 R. Srinivasan, *et al.*, *J. Electrochem. Soc.*, 2020, **167**(2), 020559.
123 S. Mousavi, *et al.*, *Appl. Therm. Eng.*, 2021, **197**, 117398.
124 A. Wazeer, *et al.*, *Energy Nexus*, 2022, **7**, 100131.
125 W. Zhang, *et al.*, *Appl. Therm. Eng.*, 2021, **184**, 116380.
126 P. Mohtat, *et al.*, *J. Electrochem. Soc.*, 2021, **168**(10), 100520.
127 W.-S. Yoon, *et al.*, *Electrochem. Commun.*, 2006, **8**(8), 1257.
128 G. Bree, *et al.*, *RSC Adv.*, 2023, **13**(10), 7045.
129 W. Jiang, *et al.*, *CCS Chem.*, 2023, **5**(6), 1308.
130 J. H. Ryu, *et al.*, *Electrochem. Solid-State Lett.*, 2004, **7**(10), A306.
131 M. Janvrin and A. Grillet, *Strain and Conductivity in Lithium Ion Battery Binders*, Sandia National Lab. (SNL-NM), Albuquerque, NM (United States), 2016.
132 U. Janakiraman, *et al.*, *J. Electrochem. Soc.*, 2020, **167**(16), 160552.
133 F. Liu, *et al.*, *Nature*, 2021, **600**(7890), 659.
134 G. Zhang, *et al.*, *ACS Appl. Energy Mater.*, 2022, **5**(5), 6462.
135 L. Fang, *et al.*, *Energy Environ. Sci.*, 2023, **16**, 3053–3062.
136 W. Yin, *et al.*, *Nat. Commun.*, 2020, **11**(1), 1252.
137 A. Grenier, *et al.*, *J. Am. Chem. Soc.*, 2020, **142**(15), 7001.
138 M. K. Aslam, *et al.*, *Nano Energy*, 2021, **86**, 106142.
139 C. D. Fincher, *et al.*, *Joule*, 2022, **6**(12), 2794.
140 L. Meyer, *et al.*, *J. Electrochem. Soc.*, 2021, **168**(9), 090502.
141 H. M. Barkholtz, *et al.*, *J. Power Sources*, 2019, **435**, 226777.
142 Y. P. Yang, *et al.*, *Polymers*, 2021, **13**(5).
143 M. S. Hosen, *et al.*, *iScience*, 2021, **24**(2), 102060.
144 S. Käbitz, *et al.*, *J. Power Sources*, 2013, **239**, 572.
145 S. Tamilselvi, *et al.*, *Sustainability*, 2021, **13**(18), 10042.